SANDIA REPORT
SAND2009-4419
Unlimited Release
Printed July 2009

Issues Associated with the Metalorganic Chemical Vapor Deposition of ScGaN and YGaN Alloys

D. D. Koleske, J. R. Creighton, S. R. Lee, M. H. Crawford, G. Thaler,
K. C. Cross, and J. A. Knapp

Prepared by
Sandia National Laboratories
Albuquerque, New Mexico 87185 and Livermore, California 94550

Sandia is a multiprogram laboratory operated by Sandia Corporation,
a Lockheed Martin Company, for the United States Department of Energy's
National Nuclear Security Administration under Contract DE-AC04-94AL85000.

Approved for public release; further dissemination unlimited.

Issued by Sandia National Laboratories, operated for the United States Department of Energy by Sandia Corporation.

NOTICE: This report was prepared as an account of work sponsored by an agency of the United States Government. Neither the United States Government, nor any agency thereof, nor any of their employees, nor any of their contractors, subcontractors, or their employees, make any warranty, express or implied, or assume any legal liability or responsibility for the accuracy, completeness, or usefulness of any information, apparatus, product, or process disclosed, or represent that its use would not infringe privately owned rights. Reference herein to any specific commercial product, process, or service by trade name, trademark, manufacturer, or otherwise, does not necessarily constitute or imply its endorsement, recommendation, or favoring by the United States Government, any agency thereof, or any of their contractors or subcontractors. The views and opinions expressed herein do not necessarily state or reflect those of the United States Government, any agency thereof, or any of their contractors.

Printed in the United States of America. This report has been reproduced directly from the best available copy.

Available to DOE and DOE contractors from
U.S. Department of Energy
Office of Scientific and Technical Information
P.O. Box 62
Oak Ridge, TN 37831

Telephone: (865)576-8401
Facsimile: (865)576-5728
E-Mail: reports@adonis.osti.gov
Online ordering: http://www.osti.gov/bridge

Available to the public from
U.S. Department of Commerce
National Technical Information Service
5285 Port Royal Rd
Springfield, VA 22161

Telephone: (800)553-6847
Facsimile: (703)605-6900
E-Mail: orders@ntis.fedworld.gov
Online order: http://www.ntis.gov/help/ordermethods.asp?loc=7-4-0#online

SAND 2009-4419
Unlimited Release
Printed July 2009

Issues Associated with the Metalorganic Chemical Vapor Deposition of ScGaN and YGaN Alloys

D. D. Koleske, J. Randall Creighton
Advanced Material Sciences Department

S. R. Lee, M. H. Crawford
Semiconductor Material & Device Sciences Department

G. Thaler, K. C. Cross
Advanced Material Sciences Department

and

J. A. Knapp
Radiation-Solid Interactions Department

Sandia National Laboratories
P.O. Box 5800
Albuquerque, New Mexico 87185-1086

Abstract

We report on issues associated with the metalorganic chemical vapor deposition growth of ScGaN and YGaN. Based on the proposed bandgaps of ScN (2.15 eV), YN (0.8 eV) and the known bandgap of GaN (3.4 eV), we expected that LEDs could be fabricated from the UV (410 nm) to the IR (1600 nm), resulting in LED over all visible wavelengths for solid state lighting However, due to the low volatility of scandium and yttrium metalorganic precursors, we were only able to incorporate doping level concentrations of these atoms into a GaN film. This report highlights the difficulties encountered during the growth of these alloys and how some of these difficulities were overcome. We also investigated the nitridation of thin scandium metal films deposited on GaN using pulsed laser deposition. GaN was also grown on these thin ScN films to as a means to lower the GaN dislocation density.

This page has been left intentionally blank

Extended Abstract

The most energy efficient solid state white light source will likely be a combination of individually efficient red, green, and blue LED. For any multi-color approach to be successful the efficiency of deep green LEDs must be significantly improved. While traditional approaches to improve InGaN materials have yielded incremental success, we proposed a novel approach using group IIIA and IIIB nitride semiconductors to produce efficient green and high wavelength LEDs.

To obtain longer wavelength LEDs in the nitrides, we attempted to combine scandium (Sc) and yttrium (Y) with gallium (Ga) to produce ScGaN and YGaN for the quantum well (QW) active regions. Based on linear extrapolation of the proposed bandgaps of ScN (2.15 eV), YN (0.8 eV) and GaN (3.4 eV), we expected that LEDs could be fabricated from the UV (410 nm) to the IR (1600 nm), and therefore cover all visible wavelengths. The growth of these novel alloys potentially provided several advantages over the more traditional InGaN QW regions including: higher growth temperatures more compatible with GaN growth, closer lattice matching to GaN, and reduced phase separation than is commonly observed in InGaN growth. One drawback to using ScGaN and YGaN films as the active regions in LEDs is that little research has been conducted on their growth, specifically, are there metalorganic precursors that are suitable for growth, are the bandgaps direct or indirect, can the materials be grown directly on GaN with a minimal defect formation, as well as other issues related to growth.

The major impediment to the growth of ScGaN and YGaN alloys was the low volatility of metalorganic precursors. Despite this impediment some progress was made in incorporation of Sc and Y into GaN which is detailed in this report. Primarily, we were able to incorporate up to 5×10^{18} cm^{-3} Y atoms into a GaN film, which are far below the alloy concentrations needed to evaluate the YGaN optical properties.

After a no-cost extension was granted on this program, an additional more “liquid-like” Sc precursor was evaluated and the nitridation of Sc metals on GaN were investigated. Using the Sc precursor, dopant level quantities of Sc were incorporated into GaN, thereby concluding the growth of ScGaN and YGaN films. Our remaining time during the no-cost extension was focused on pulsed laser deposition of Sc metal films on GaN, followed by nitridation in the MOCVD reactor to form ScN. Finally, GaN films were deposited on the ScN thin films in order to study possible GaN dislocation reduction.

Acknowledgments

We acknowledge Jeff Figiel and Mike Russell for their daily technical contributions to the growth and characterization of nitride based films grown in this program, routine maintenance of the MOCVD growth equipment, and for preparation of the D125 MOCVD reactor for the move to the new MESA facility which occurred midway during this research project.

Sandia is a multiprogram laboratory operated by Sandia Corporation, a Lockheed Martin Company. This work is supported by the Division of Material Science, Office of Basic Energy Science for the United States Department of Energy's National Nuclear Security Administration under Contract DE-AC04-94AL85000.

Contents

Title and Authors 3
Abstract 3
Extended Abstract 5
Acknowledgements 5
Contents 6
Figures List 7
Tables List 9
Nomenclature 10
0. Executive Summary 11
1. Project Objective 11
2. Project Background 12
2.1. Status of InGaN alloy growth for green and longer wavelength LEDS 12
2.2. Potential of ScGaN and YGaN alloys for longer wavelength LEDs 15
3. Comparison of actual accomplishments to proposed goals 18
3.1. Project milestones 18
3.2. Tasks to meet program goals and actual program accomplishments......19
3.3. Tasks developed for no-cost extension and actual accomplishments 21
4. Summary of project activities 22
4.1. Task 1 summary 22
Milestone 1.1 - summary 22
Milestone 1.2 - summary 24
Milestone 1.3 - summary 24
Milestone 1.4 - summary 30
Milestone 1.5 - summary 30
4.2. Tasks performed under the no-cost extension 30
4.3. Work performed in support of all tasks 34
5. Summary of project activities 34
6. References 35
7. Appendix A 37
8. Appendix B. Brief Project Award Information 39
Distribution List 40

Figures List

1. Depicts overall project goal. In (a), the external quantum efficiency (EQE) and internal quantum efficiency (IQE) for Lumileds Luxeon LEDs are plotted as a function of the emitting wavelength [From Ref. 1, 2, and 5]. The Group III nitrides are (blue lines) used for LEDs emitting at wavelengths less than 550 nm, the Group III phosphides (red lines) are used for LEDs emitting at wavelengths greater than 550 nm. Our goal as shown in (b) where scandium (Sc) and Yttrium (Y) are added to the InGaN quantum wells to shift the more efficient LEDs at 460 nm to longer wavelengths. Two examples of this shift to longer wavelength are shown in (b), one where 50% Sc is substituted for Ga, and the other where 35% Y is substituted for Ga in the InGaN QW. If this approach is successful we should be able to achieve all visible colors of LEDs with IQEs similar to near UV and blue InGaN-based LEDs 11

2. XRD measurements of the composition of 100 nm thick InGaN films grown on GaN at 760 °C. Initially coherent $In_xGa_{1-x}N$ films are limited to x=0.20 at high TMIn flow rates. Strain relaxation occurs as the film grows thicker, which yields a second layer with much greater In content at the same high flow rates 12

3. A pair of HRTEM lattice fringe images showing (a) an undamaged and (b) an electron beam damaged after minutes of exposure of an $In_{0.22}Ga_{0.78}N$ quantum well. In (c) and (d) the lattice parameter maps extracted from the images are shown. From Ref. [**Error! Bookmark not defined.**] 12

4. Plot of the growth temperatures typically used for InGaN growth along with the indium contents (fraction) needed to achieve violet, blue, green, and yellow wavelengths. Also plotted are the binodal and spinodal phase separation calculated by Ho and Stringfellow [11] 13

5. The bandgap shift for ScGaN alloys plotted as a function of the % scandium [30]. This plot demonstrates that ScGaN alloys can be grown over the entire alloy range 16

6. Plot of the estimated wavelengths expected for ScGaN and YGaN alloys based on linear extrapolation of the bandgaps for GaN (3.4 eV), ScN (2.15 eV), and YN (0.8 eV) 16

7. NMR spectra of the tris-methylcyclopentadienylyttrium, $(Mecp)_3Y$. Hydrogen peaks from the cyclopentadienyl ring (labeled H') occur near 5.9 ppm and hydrogen peaks form the methyl groups (labeled H) occur near 2.0 ppm. From the NMR, the material does not show any organic impurities. There is some oxygen species in <100 ppm concentration 21

8. Thermogravimetric analysis (TGA) of the yttrium precursor. The TGA analysis indicated a very clean material with a low residue of < 5 %, while residue due to the yttrium metal alone would have been around 27 % 22

9. Vapor pressure curves vs. temperature for the $(Mecp)_3Y$ compound (open and filled squares and black solid line) and other common metalorganic precursors used for growth and doping of the group III nitrides 22

10. UV absorption of magnesium (blue circles), gallium (red squares) and yttrium (green diamonds) precursors. The vapor pressures of the magnesium and yttrium precursors are similar and should yield similar absorption signals 24

11. The UV transmission through the UV cell is plotted as a function of time for different bubbler flow rate conditions with the bubbler both open and closed. The bubbler loop pressure was held at 600 torr and bubbler temperature at 50.7 °C. Note that once the

bubbler is first opened there is a larger decrease in the UV transmission due to an increase in the absorption from the cyclopentadienyl groups flowing through the UV cell. Flow conditions ranged from 50 to 800 cubic centimeters (cc) per minute 25

12. Using the UV transmission data, the product of the UV absorption and the flow rate through the bubbler is plotted vs. the flow rate. This product should be proportional to the molar flow rate out of the bubbler. If the precursor saturates the gas phase then the ideal behavior is observed and the molar flow rate depends linearly on the flow rate through the bubbler. However if the precursor does not saturate the vapor phase then the molar flow rate will be sub-linear as shown by the data in red 26

13. Optical reflectance waveform at 550 nm (red) and 400 nm (blue) for an attempt at YGaN alloy growth. The decrease in the optical reflectance signal is due to surface roughening which is induced via the introduction of the yttrium precursor 27

14. Nomarski phase contrast images of the roughened film produced when the yttrium precursor is introduced during GaN growth. The objective magnification for each of the images is (a) x50, (b), x50, and (c) x100. The hexagonal symmetry is expected of wurtzite material and may occur due to yttrium or impurity induced re-nucleation on the original GaN surface 27

15. Secondary ion mass spectroscopy (SIMS) of yttrium (orange open circles) incorporation in GaN. The GaN substrate was silicon (red open squares) doped so that the interface between the GaN substrate and the yttrium doped region could be clearly discerned. The yttrium concentration reaches a level of $5.3x10^{18}$ cm^{-3} for a thickness of ~0.6 m 28

16. Secondary ion mass spectroscopy (SIMS) depth profile for the element scandium of sample grown using the liquid scandium precursor. On top of a GaN template scandium was introduced at a slower GaN growth rate to increase the level of scandium in the GaN. A GaN capping was grown on top of the scandium doped GaN layer to eliminate SIMS surface effects on the scandium concentration measurement 29

17. (a) Photographs of Sc-metal films deposited on GaN/sapphire quarter-wafer templates; the photos are taken before and after nitridation in NH3 at 1050 °C. (b) SEM/EDS spectra taken near the center of each of the three samples. The Sc Ka peaks near 4.09 keV have similar intensities before and after nitridation indicating that the samples do not lose Sc during nitridation 30

18 (a) Sample photograph and (b-d) SEM images of GaN grown on 16-nm-thick ScN layers on top standard GaN/sapphire templates using a two-step nucleation and growth procedure. GaN is nucleated at temperature T_1=900 ^oC for 15 minutes, and then temperature is ramped to T_2=1050 ^oC for an additional 60 minutes of growth. Numbered labels in panel (a) indicate the positions where SEM images were taken.......... 31

19 Nomarski optical microscopy of the growth surface of coalesced, 2-μm-thick GaN regrown on thin ScN interlayers (200X magnification via eyepiece). Labeled Sc-film thicknesses are for the as-deposited metal film prior to nitridation and regrowth 32

Tables List

1. Lattice constants for group-III nitride alloys. 15
2. Diatomic bond energies. 15
3. Project Milestones and Completions Dates.. 18

Nomenclature

AFM	atomic force microscopy
AlN	aluminum nitride
DOE	Department of Energy
EDS	energy dispersive x-ray
EQE	external quantum efficiency
eV	electron volt
GaN	gallium nitride
H_2	hydrogen gas
H_20	water
HBA	hazard barrier analysis
InN	indium nitride
IQE	internal quantum efficiency
LED	light emitting diode
moles	micromoles
m	micrometer
$(Mecp)_3Y$	tris-methylcyclopendadienyl-yttrium
MOCVD	metalorganic chemical vapor deposition
MQW	multiple quantum wells
NH_3	ammonia gas
N_2	nitrogen gas
$(n\text{-}Bucp)_3Sc$	tris-n-butylcyclopendadienyl-scandium
$(n\text{-}Bucp)_3Y$	tris-n-butylcyclopendadienyl-yttrium
nm	nanometer
NMR	nuclear magnetic resonance
PL	photoluminescence
PLD	pulsed laser deposition
ppm	parts per million
RBS	Rutherford backscattering
RMS	root-mean-square
SEM	scanning electron microscope
ScGaN	scandium gallium nitride
ScN	scandium nitride
sccm	standard cubic centimeters per minute
Si	elemental silicon
SIMS	secondary ion mass spectroscopy
SLM	standard liters per minute
SNL	Sandia National Laboratories
SS	stainless steel
SSL	solid state lighting
TEM	transition electron microscopy
TGA	thermogravimetric analysis
TMGa	trimethylgallium
UV	ultra-violet
XRD	x-ray diffraction
YGaN	yttrium gallium nitride
YN	yttrium nitride

0. Executive Summary

One long-term, highly-efficient approach to solid state white lighting is to combine efficient red, blue, and green LEDs. For this approach to be successful dramatic improvements are needed to improve the luminous efficiency of green LEDs. One of the possible reasons for the green LED efficiency decrease is because as indium is added to the InGaN multi-quantum well (MQWs) the material quality decreases, due to the lower growth temperature (700-770 ºC) necessary to incorporate indium. At these lower growth temperatures, higher ammonia flows are also necessary to compensate for the decreased ammonia dissociation efficiency. In addition, strain between the InGaN and GaN layers limits the amount of indium which can be incorporated to ~ 20 %.

To overcome these obstacles for producing efficient green LEDs, we proposed to introduce scandium and yttrium into GaN MQWs of LEDs. The bandgaps ScN and YN have been proposed to be 2.15 eV [1] and 0.8 eV [2], respectively, so that ScGaN and YGaN alloys should cover the same wavelength range as InGaN, i.e. from 364 to ~1500 nm.

However, unlike the Group IIIB nitrides (InAlGaN), almost no work has been done on ScN and YN growth, especially using a more commercial growth technique such as metalorganic chemical vapor deposition (MOCVD). In terms of growth there are several possible advantages of growing ScGaN and YGaN including the possibility of using temperatures typically used for GaN (~1050 ºC) growth, the possibility of using less ammonia than what is used for InGaN growth, and the possibility of reducing the tendency for phase separation typically observed InGaN. Also, because Sc and Y are closer than indium to Ga in the periodic table, the ScN and YN lattice constants should more closely match GaN than InN.

Several issues arose after the start of this program due to the complexity of growing these novel materials. The primary issue was the low volatility of the Sc and Y metalorganic precursors, making them incompatible with traditional MOCVD growth of the group-III nitrides. Using cyclopentadienyl substituted Sc and Y precursors we were able to achieve doping level quantities of Sc and Y into GaN; however these low doping levels were several orders of magnitude lower than what is needed for alloy formation. Details of chemical precursors used and the modifications to the growth needed to achieve doping level quantities of Sc and Y into GaN are highlighted in this report.

After the first year review, a no-cost extension was granted and the program focus shifted from using MOCVD to grow ScGaN and YGaN alloys to nitriding deposited Sc metal films on GaN. During this time, we demonstrated that the Sc metal films could be nitrided; however they showed no luminescence that would indicate a lower bandgap than GaN. We also grew GaN films on the ScN films to determine if the ScN films could be used for dislocation reduction as reported in the literature. Some success was achieved in getting GaN to coalesce on the ScN film; however details of the possible dislocation reduction are still under investigation. We acknowledge that this research was very exploratory and high risk but believed that it fit well with the EERE/NETL call to develop *high efficiency materials systems* that produce *orange, yellow, and green radiant emission*.

1. Project Objective

To overcome obstacles to high-brightness green and longer wavelength LEDs, we proposed to develop scandium nitride (ScN) and yttrium nitride (YN) materials and incorporate them into the active regions of InGaN QWs. The ScN and YN bandgaps have been theoretically studied and experimentally measured to be around 2.15 eV [1] and 0.8 eV [2], respectively, so that ScGaN and YGaN alloys should cover the same wavelength range as InGaN, i.e. from 364 to ~1500 nm. *This proposal's overall goal of this research was to red-shift the wavelength of the most efficient*

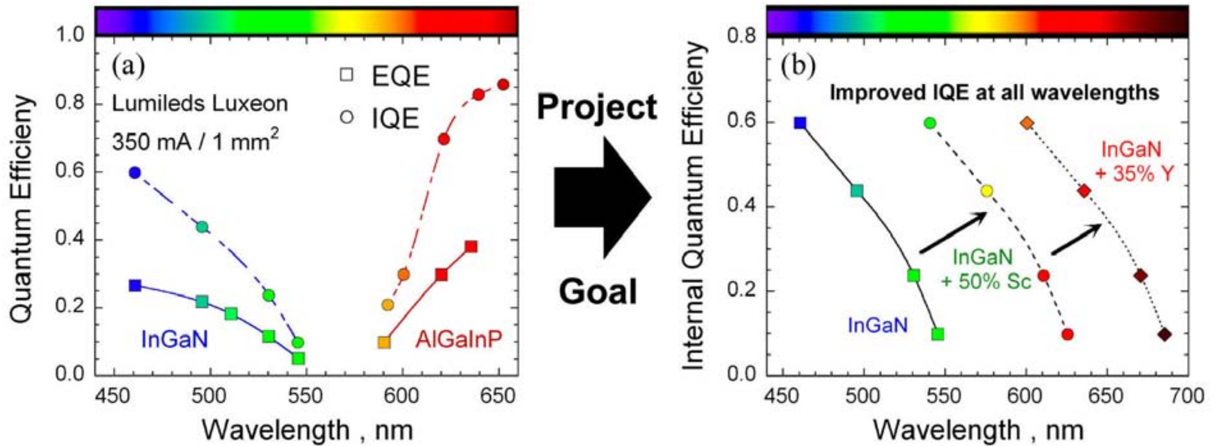

Fig. 1 Depicts overall project goal. In (a), the external quantum efficiency (EQE) and internal quantum efficiency (IQE) for Lumileds Luxeon LEDs are plotted as a function of the emitting wavelength [From Ref. 1, 2, and 5]. The Group III nitrides are (blue lines) used for LEDs emitting at wavelengths less than 550 nm, the Group III phosphides (red lines) are used for LEDs emitting at wavelengths greater than 550 nm. Our goal as shown in (b) where scandium (Sc) and Yttrium (Y) are added to the InGaN quantum wells to shift the more efficient LEDs at 460 nm to longer wavelengths. Two examples of this shift to longer wavelength are shown in (b), one where 50% Sc is substituted for Ga, and the other where 35% Y is substituted for Ga in the InGaN QW. If this approach is successful we should be able to achieve all visible colors of LEDs with IQEs similar to near UV and blue InGaN-based LEDs.

InGaN-based LEDs in the near UV and blue to longer wavelengths in the green, yellow, and orange by adding Sc and Y to the QWs. If this approach would have been successful, efficient LEDs could have been available at all visible wavelengths.

This overall goal is depicted in Fig. 1. The internal quantum efficiency (IQE) and the external quantum efficiency (EQE) are shown in Fig. 1(a) as a function of increasing wavelength for nitride-based (left) and phosphide-based (right) LEDs. The proposed increase in the IQE with the addition of Sc and Y to the InGaN QWs is shown in Fig. 1(b). In Fig. 1(b), theoretical wavelength shifts and subsequent IQEs are estimated from Fig. 1(a) for LEDs with InScGaN QWs (50% Sc) or InYGaN QWs (35% Y).

2. Project Background

2.1. Status of InGaN growth for green and longer wavelength LEDs.

With bandgaps that span ~ 0.8 eV (InN) [3] to 3.4 eV (GaN), all visible colors should be achievable using InGaN alloys. However, as observed in Fig. 1(a), the IQE and EQE of nitride LEDs decreases sharply as indium is added to the QWs to increase the emission wavelength. Nitride-based yellow and red LEDs have been demonstrated however the light emission from these LEDs is small compared to the light emission from blue and green LEDs [4]. The decrease in the emission intensity for green and longer wavelength LEDs in the nitrides is most likely due to the poor InGaN material quality as the indium content increases.

Two major issues are believed to limit the InGaN material quality. These issues are the increased strain as the indium content is increased and the low InGaN growth temperature that must be used to incorporate the indium. Both of these issues are discussed in the subsequent paragraphs along with their impact on the reduced light output in nitride LEDs.

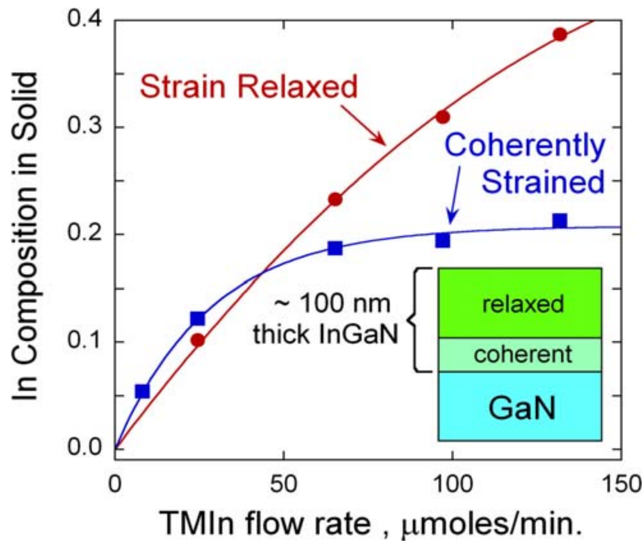

Fig. 2. XRD measurements of the composition of 100 nm thick InGaN films grown on GaN at 760 °C. Initially coherent $In_xGa_{1-x}N$ films are limited to x=0.20 at high TMIn flow rates. Strain relaxation occurs as the film grows thicker, which yields a second layer with much greater In content at the same high flow rates.

As the indium content increases, the lattice-mismatch strain between the InGaN and GaN increases. Recently, we have observed the effect of strain on limiting indium incorporation in thick ~100 nm InGaN layers grown on GaN. In Fig. 2 the indium composition in the InGaN is plotted vs. the indium metalorganic (MO) flow rate with the NH_3 and Ga MO flows held constant. The indium content in the solid was measured using XRD scans of the (0004) and ($10\underline{1}2$) reflections. As the InGaN film is deposited it initially forms a coherent layer on the GaN and this coherent InGaN layer is limited to an indium composition of ~20%. As the InGaN layer grows thicker, the InGaN strain-relaxes and can incorporate more indium; up to 40% indium for the highest indium flow rate for the highest indium flow conditions shown in Fig. 2. The coherent strain state of 3.0 nm thick, 20% indium concentration, InGaN multi-quantum wells (MQWs) was confirmed using an XRD k-space map of the ($20\underline{2}5$) reflection. If the strain limited indium concentration is limited to 20 %, which is sufficient to generate green colors on c-plane substrates, it might be difficult to achieve wavelengths longer than green unless the InGaN material can be strain relaxed. Since defects such as dislocations have to be introduced to relax strain, the light output in these higher indium concentration layers will most likely be reduced.

For example, we have used 20 % indium concentration InGaN QWs to fabricate green LEDs. The measure light output for 521 nm LED was 1/3 the light output of a 500 nm LED and 1/9 that of a 423 nm LED. This decrease in the LED output as the wavelength is increased demonstrates a commonly observed trend for nitride-based LEDs shown in Fig. 1(a) and in Ref. [**Error! Bookmark not defined.**].

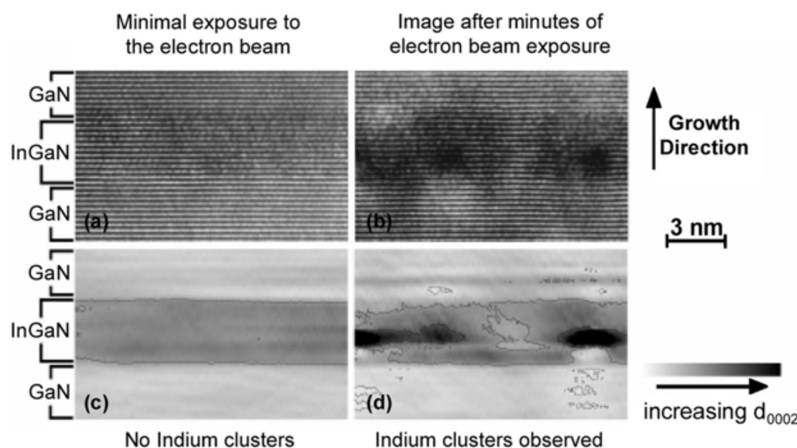

Fig. 3 A pair of HRTEM lattice fringe images showing (a) an undamaged and (b) an electron beam damaged after minutes of exposure of an $In_{0.22}Ga_{0.78}N$ quantum well. In (c) and (d) the lattice parameter maps extracted from the images are shown. From Ref. [**Error!**

As shown in Ref. [**Error! Bookmark not defined.**] and to some degree in Fig. 1(a), the LED power output increases, peaks near 10% indium concentration and then decreases as indium is added to the QWs. One explanation for this initial increase and subsequent decrease involves indium localization within the QWs. For pure GaN the non-radiative recombination is very effective and it appears to be less effective for low indium composition InGaN. When more indium is added localized "quantum dot-like" structures form and the minority carriers become increas-

ingly localized in In-rich quantum wells and the trapping of carriers at the abundant threading dislocations or other nonradiative recombination centers decreases [5]. However as the indium content increases to 15-20 % and the localization increases, these "quantum dot-like" structures may have increased defect structure, which will again increase non-radiative recombination leading to reduced light emission from the QWs.

However, recent experimental investigations of InGaN MQWs bring into question this viewpoint as to whether or not these indium-rich "quantum dot" are even formed at all and whether they are even beneficial for green LEDs [6-9]. For instance TEM observations from Smeeton *et al.* the indium appears to be laterally uniform as shown in Figs. 3(a) and 3(c) [7]. For these QWs the indium content was 22% as measured by XRD which is close to the limiting indium content for coherently strained layers as shown in Fig. 2. During electron beam exposure, indium clusters can be formed if the QW is exposed to the electron beam long enough as shown in Figs. 3(b) and 3(d) [7]. The study by Smeeton *et al.* may explain why indium "quantum-dot" formation is so frequently observed in TEM observations of QWs. It is because the imaging conditions cause the observation of "quantum-dots". In another study the smoothness of the InGaN and GaN interfaces was optimized resulting in an improved green LED output power [6]. Both of these results suggest that it is not the decreased emission from localized "quantum-dot" structure that limit the green light emission, but rather the limitations due to increased defects in the InGaN material [8]. In our laboratory, increased defect content in green LED wafers can be observed in the yellowish appearance after growth. Also if we lower the growth temperature by only 2-5 ºC, the wafers have a grayish appearance suggesting metallic indium is incorporated. In fact the indium metal lattice constant is 3.252 Å [10], which is closer to the GaN lattice constant than a relaxed 20% InGaN layer (see Table 1 below). Each of these results suggests that better quality InGaN is needed for improved green LEDs.

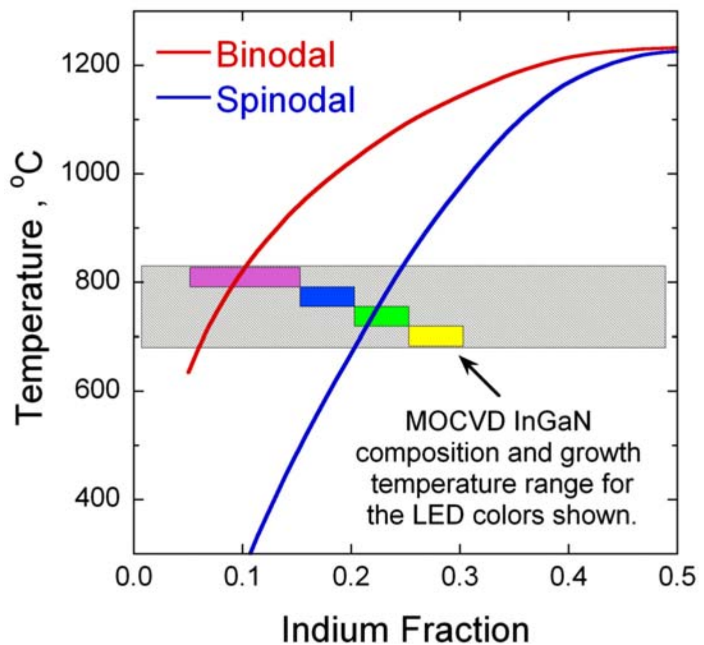

Fig. 4. Plot of the growth temperatures typically used for InGaN growth along with the indium contents (fraction) needed to achieve violet, blue, green, and yellow wavelengths. Also plotted are the binodal and spinodal phase separation calculated by Ho and Stringfellow [11].

We now consider the consequences of the low growth temperature on green InGaN QWs. Typical growth temperatures for violet, blue, green, and yellow LEDs are shown in Fig. 4, along with the approximate indium compositions needed to achieve these wavelengths. Also shown in Fig. 4 are the binodal and spinodal phase separation calculations by Ho and Stringfellow, which suggest that at 800 ºC the solubility of indium in GaN should only be 6% [11]. The phase separation calculations show that the InGaN films are at best metastable, and may decompose if subjected to high temperature anneals [12] or the higher p-side growth conditions required for better quality p-type GaN.

As the InGaN growth temperature is decreased, the growth quality could possibly decrease for several reasons. First the NH_3 catalytic dissociation efficiency decreases exponentially with temperature. To compensate for the decreased NH_3 dissociation rates, the NH_3 flow rates for

InGaN growth are increased. Also, because the NH_3 must be catalytically dissociated on the surface, changing from a Ga-rich to an In-rich surface might further decrease the NH_3 dissociation efficiency due to the reduced ionic nature of the surface [13]. Second, at these lower growth temperatures, point defects may form in greater densities due to the reduced adatom mobility [13]. Third, the lower growth temperature will increase the carbon and hydrogen impurities in the GaN and InGaN [14, 15] with carbon coming from the dissociation of the methyl groups from the metalorganic precursors and hydrogen coming from incomplete NH_3 dissociation and C-H moieties. At the high temperatures used for GaN growth chemical pathways exist for carbon rehydrogenation [15]. Both point and impurity defects likely contribute to the yellowish color of green LEDs wafers while GaN wafers grown at high temperature are typically colorless and transparent, as expected from a semiconductor with a bandgap of 3.4 eV. The yellowish wafer color suggests an increase in defect density which should decrease the overall radiative efficiency of the InGaN QWs. Carbon is a known electron trapping type defect in GaN material [16], and has been shown to electrically compensate n-type GaN material to the point that it becomes insulating [17].

Finally, the temperature stability of the high indium content InGaN films during Mg activation and final contact annealing may also be an issue. Lower growth temperature p-type GaN is needed to prevent decomposition of the green InGaN QWs [12]. While these lower growth temperatures enable green LEDs, the quality of the p-type GaN is reduced and this material likely has more incorporated carbon and hydrogen. The potential fragility of the InGaN QWs puts limits on the Mg activation in GaN [18], as well as the thermal processing anneals for ohmic contacts layers.

2.2. Potential of ScGaN and YGaN alloys for longer wavelength LEDs.

In this section we highlight potential advantages and challenges associated with using ScGaN and YGaN alloys in the active regions of nitride-based LEDs. These advantages were discussed in the original proposal and are described here to motivate the proposal. Unfortunately, because of the difficulty in delivering the metalorganic precursors, many of these potential advantages were never realized or tested.

Some of the possible advantages for developing ScGaN and YGaN alloys include higher growth temperatures, better lattice matching, growth chemistry that is more compatible with GaN growth, and the possibility of light emission at all visible wavelengths. However, unlike the conventional AlInGaN materials, there have only been a handful of reports on the growth of ScN, YN, and alloys with GaN and there are many challenges associated with the growth of these materials, including availability of metalorganic precursors, compatibility with the nitride reactor environment, whether the bandgap transitions are direct or indirect, and preference for the rocksalt crystal structure. Each of these advantages and challenges are discussed in this section.

Unlike the lower growth temperature (700-770 °C) necessary for InGaN growth, ScN and YN are refractory nitrides which can be grown at high temperatures [19]. This means that the ScGaN and YGaN alloys can be grown at temperatures (1000 – 1100 °C) compatible with GaN growth. This will be the most significant advantage of ScGaN and YGaN alloys in regard to the growth of green and longer wavelength LEDs. Higher temperature growth should reduced the point defect concentrations inherent in the low temperature InGaN growth and bring the growth "closer to equilibrium" [13]. Also unlike InGaN which can only be grown in N_2, ScGaN and YGaN can likely be grown in H_2 and the alloys should be thermodynamically stable, unlike InGaN. The addition of H_2 during alloy growth should reduce the impurity content [15]. In addition, the NH_3 dissociation on the nitride surface should be substantially greater so that N vacancies should be reduced and the possibility of metallic inclusions reduced. Carbon and hydrogen content should also be reduced at these higher growth temperatures [14, 15]. By

Table 1. Lattice constants for group-III nitride alloys

Material	Lattice type	*a*-lattice const. Å	(0001) or (111) *a*-lattice const. Å	a/a_{GaN}	reference
GaN	Wurtzite	3.189	3.189	1.000	[19]
ScN	Rocksalt	4.50	3.183	0.998	[20]
YN	Rocksalt	4.88	3.45	1.081	[21]
InN	Wurtzite	3.57	3.57	1.120	[20]
In metal	Tetragonal	3.252	3.252	1.020	[10]
$In_{0.20}Ga_{0.80}N$	Wurtzite	relaxed	3.265	1.024	[22]
$Sc_{0.50}Ga_{0.50}N$	?	-	3.186	0.999	[22]
$Y_{0.50}Ga_{0.50}N$	?	-	3.320	1.041	[22]

reducing the point defect and impurity concentration in the active regions, the radiative efficiency of the LEDs should be increased over the current efficiency observed in the low temperature InGaN green LEDs.

The lattice constants and preferred lattice types of the relevant nitride alloys are shown in Table 1 [10, 19-22]. The energy difference between the rocksalt and wurtzite lattices is smaller for ScN and YN than for GaN suggesting that the ScGaN and YGaN might favor the wurtzite lattice [23]. In fact, theoretical calculations suggest that the hexagonal phase of ScN is only 316 meV higher in total energy than the ground-state rocksalt phase, while the GaN rocksalt phase is 887 meV higher in total energy than the ground-state wurtzite phase [24]. This implies that if ScN is alloyed with GaN, the energy difference is likely to favor forming the wurtzite crystal structure over the rocksalt structure [23]. However, experimental evidence for ScGaN (or YGaN) mixing in the wurtzite phase is currently lacking and would need to be verified in the first year of this proposal.

Table 2. Diatomic bond energies

Element M	Diatomic Bond Energy with M-M (eV) [26]	Diatomic Bond Energy with M-N (eV) [26]
Al	1.38 ± 0.06	3.1 ± 1
Sc	1.69 ± 0.22	4.9 ± 0.9
Ga	1.40 [28]	2.5 ± 1 [28]
Y	1.62 ± 0.26	5.0 ± 0.6
In	1.04 ± 0.06	~ 2 ± 1

Since Sc and Y are closer to Ga on the periodic table than In is, their nitrides have closer in-plane lattice constants to GaN than InN as calculated in column 5 of Table 1. The lattice constants for GaN and InN are for the wurtzite lattice while the lattice constant for ScN and YN are for the rocksalt lattice. For example, the *a*-axis lattice constant for GaN and ScN are within 0.2 % of one another, suggesting that strain in the ScGaN alloys will be minimal. YN has an 8% lattice mismatch to GaN but this mismatch is smaller than the InN 12% lattice mismatch to GaN. While the difference in preferred lattice type may appear to be a major problem with the growth of these alloys, the close lattice match and high temperature stability of these materials suggest that ScGaN might retain the wurtzite lattice [24]. In fact, ScGaN compounds have been fabricated over the entire range from GaN to ScN as shown in Fig. 5, demonstrating that mixed alloys are possible [25]. However for this study the crystal structure was not reported and crystal quality was likely poor based on the crystal sputtering growth method [25].

Another advantage of ScGaN and YGaN alloys are that Sc and Y have chemistry more similar to Al and Ga than does indium. In particular, the chemistry of Sc closely matches that of Al [26]. This is an advantage for the growth of ScGaN and YGaN alloys since there has been much

recent work on the growth of high quality AlGaN for deep UV emitters [27]. Comparisons of the metal-metal diatomic bond energy and the diatomic bond energy with nitrogen are shown in Table 2 [26, 28]. Note that the metal-metal bond energies are shown in column 2 of Table 2. Note that the metal-metal (M-M) bond energies for Al, Sc, Ga, and Y are close to one another with the In metal-metal bond energy being somewhat lower. In the third column of Table 2 the diatomic bond energies with N (M-N) are listed with both Sc-N and Y-N bond energies near 5 eV and Al-N and Ga-N near 2.5 to 3.0 eV. For Table 2, In-N bond energy had to be estimated based on the bond energies of In with the other group V elements. Because the metal-metal bond energies of Al, Sc, Ga, and Y are similar, we expect the surface diffusion barriers and incorporation kinetics of ScGaN and YGaN to be similar to AlGaN.

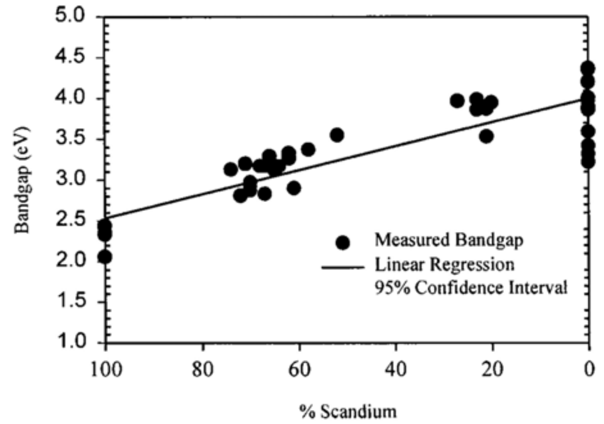

Fig. 5 The bandgap shift for ScGaN alloys plotted as a function of the % scandium [**Error! Bookmark not defined.**]. This plot demonstrates that ScGaN alloys can be grown over the entire alloy range.

Another issue associated with the growth of ScGaN and YGaN will be the precursor delivery and the choice of precursor. These difficulties are discussed in more detail later in the report. Yet another potential issue with the growth of the ScGaN and YGaN alloys is that gas phase adduct and cluster formation may decrease the amount of Sc and Y that can reach the surface. Recently, Creighton *et al.* studied adduct and cluster formation for GaN and AlN and found that different reaction mechanisms may contribute to Ga and Al cluster formation [29]. One finding from this study is that the cluster formation and precursor depletion reaction rates can be decreased by reducing the metal flow and this has recently been demonstrated by Allerman *et al.* for AlGaN growth [27]. A lower total MO flow rate may be necessary for ScGaN and YGaN growth because of the low vapor pressure expected from the Sc and Y precursors.

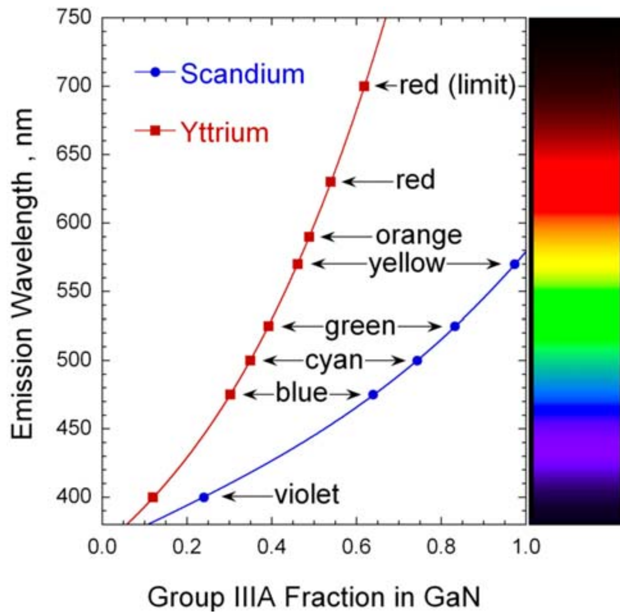

Fig. 6. Plot of the estimated wavelengths expected for ScGaN and YGaN alloys based on linear extrapolation of the bandgaps for GaN (3.4 eV), ScN (2.15 eV), and YN (0.8 eV).

With there being favorable temperature compatibility, lattice matching and chemical compatibility, ScGaN and YGaN are potentially suited to replace InGaN as the active layers in LEDs, provided the bandgaps follow what has been reported in the literature. The bandgap of ScN has been established around 2.1 to 2.4 eV as shown in Fig. 5, with 2.15 eV being the most widely accepted [30-33]. Theoretical calculations of ScN in the wurtzite phase have suggested a higher bandgap near 3 eV [34]. Recent calculations by Ranjan *et al.* suggest that if the ScN lattice is compressed from 3.4% to 6.4% the bandgap spans the entire range of the visible light spectrum [35]. The results from these calculations are very interesting in that compression of the ScN lattice could be used to vary the LED wavelength, rather than the varying the Sc or Y content in the alloy. To date the calculations of Ranjan *et*

al. have not been experimentally verified [35], however in the proposed research we will look for such shifts in the ScN emission as the lattice is compressed. Fewer studies have been reported for the bandgap of YN, which has been calculated to be ~ 0.85 eV [2]. Note that the bandgap for YN is very similar to the currently re-established bandgap of ~0.8 eV for InN [3].

Using a ScN bandgap of 2.15, a YN bandgap of 0.85 eV, and a GaN bandgap of 3.4 eV, we show the expected wavelength for ScGaN and YGaN alloys as a function of the Sc or Y alloy content in Fig. 6. For the calculation we have used linear interpolations between each of the ScN and YN bandgaps with GaN. Note that green emission should be achieved at a Sc content of 85% and a Y content of 38%, while yellow should be achieved using a ScN QW or a YGaN QW with a Y content of 45%, and orange would be achieved with a with a YGaN QW with a Y content of 50%. Although the wavelength dependence on Sc and Y content shown in Fig. 6 is only estimation, it does suggest the possibility that all visible wavelengths could be achieved using combinations of ScGaN or YGaN alloys. Because YN and InN have roughly the same bandgap, the wavelength dependence on the indium content should produce roughly the same wavelengths as YGaN, if the indium was stable in the InGaN alloy. We believe that the increased temperature stability and the more refractory nature of the ScGaN and YGaN alloys should provide a better chance for achieving the wavelength shifts shown in Fig. 6 than with InGaN alloys.

After fabricating LEDs with ScGaN and YGaN alloys, indium will be added to the QWs with the goal of increasing the light emission. As indium is added to InGaN QWs the emission intensity increases and peaks around an indium content of 10 % [4]. It is not entirely clear as to why the LED intensity increases as indium is added to the QWs however as stated in Section 8.1.C.1 it may be due to increased localization of the electron and hole wavefunctions in "quantum-like dot" structures. It is not clear if the addition of indium will also increase the light intensity of ScGaN and YGaN alloys, however if this does occur, we have estimated the possible IQEs if 50% Sc and 35% Y are added to the InGaN QWs shown in Fig. 1(a) in Fig. 1(b). Ideally, if this approach is successful, we should be able to fabricate nitride-based green LEDs with IQEs similar to what is currently achievable for blue LEDs.

3. Comparison of actual accomplishments to proposed goals

3.1. Project Milestones

A list of project milestones is given in Table 5. Two tasks are listed below, with Task 1 assigned to the first year and Task 2 assigned to the second year. In the first year ScGaN and YGaN alloys were to be developed for QW emission studies. After evaluation of the MO precursors, we intended on putting Sc and Y into our blue and green LEDs as a "proof-of-concept" to see if the wavelength red-shifts. We also intended on developing ScGaN and YGaN alloys leading up to an assessment of how much Sc or Y need to be added to achieve green, yellow, and orange LEDs. However, by not achieving Milestone 1.3, subtasks 1.2, 1.4, and 1.5 along with all subtasks in Task 2 were stopped and three different tasks were developed during the no-cost extension. Details of the subtasks and accomplishments in the first year are discussed in Section 3.B and details of the no-cost extension tasks for the second year are discussed in Section 3.C.

Table 3 – Project Milestones and Completion Dates

Task 1 – MOCVD growth of ScGaN and YGaN alloys (First Year).		
Milestone 1.1	Purchase and evaluate metalorganic scandium and yttrium sources and modify reactor- completed.	**Month 2**
Milestone 1.2	Add Sc and/or Y to conventional blue and green InGaN-based LEDs. - Achieve a wavelength shift of 20 nm without loss in output power -delayed.	Month 5
Milestone 1.3	Develop ScGaN and YGaN growth and characterization capabilities. - Achieve ScGaN alloys with 30% Sc and YGaN alloys with 10% Y – limited progress on achieving milestone.	Month 7
Milestone 1.4	Achieve ScGaN alloys with 50% Sc and YGaN alloys with 30% Y -delayed.	Month 9
Milestone 1.5	Determine PL wavelength dependence on Sc and Y contents in alloys. - Determine target Sc and Y concentration needed in alloys to achieve green, yellow, and orange LEDs - delayed.	Month 12
Task 2 – Increase brightness of InScGaN and InYGaN based-LEDs (Second Year). Changed for no-cost extension		
Milestone 2.1	Achieve ScN (100 % Sc) and YGaN alloys with 50% Y.	Month 14
Milestone 2.2	Demonstrate green (530 nm) and yellow (570 nm) LEDs using either ScGaN or YGaN active regions.	Month 17
Milestone 2.3	Demonstrate an orange (590 nm) or longer wavelength LED using YGaN active regions.	Month 20
Milestone 2.4	Add indium to the ScGaN and/or YGaN to increase the IQE. - Achieve green (530 nm), yellow (570 nm), and orange (590 nm) LEDs with an IQE similar to the best Sandia blue LEDs.	Month 24

3.2. Tasks Developed to Meet Goals and Actual Accomplishments

Below are listed five subtasks from Task 1. Following each subtask is a paragraph on the actual accomplishments made in each task, along with a description of how the accomplishments listed differed from the proposed work. Scientific details for each task are described in Section 4 in the Summary of Project Activities. The program was only funded for one year, since we were unable to successfully demonstrate significant Sc or Y incorporation into GaN. Details of the no-cost extension using the remaining first year funding are discussed in Section 3.C.

Task 1 – MOCVD growth of ScGaN and YGaN alloys (First Year).
The goal of this task will be to develop ScGaN and YGaN alloys and then use them as active layers in green and yellow LEDs. Since MOCVD work of this nature has not been attempted before, we spend the first year of this project developing ScGaN and YGaN materials. This included evaluating MO precursors, investigating the growth of ScGaN and YGaN, developing methods to characterize the Sc and Y content, and at the end of this task determining if ScGaN and YGaN alloys could be used to increase the PL emission wavelength.

Subtask 1.1 Purchase and evaluate metalorganic scandium and yttrium sources modify the reactor.
In this subtask metalorganic (MO) sources will be evaluated to determine their suitability for delivering Sc and Y into the reactor. Initially, cyclopentadienyl chemical groups will be used for delivery of the metals, however other sources might also be evaluated if necessary. The sources will be evaluated for compatibility with the reactor environment, vapor pressure (which is currently unknown), and growth rate achievable. The sources will also need to be purified for the later stages of this work, due to the high oxygen content in starting Sc and Y precursors.

Modifications to the MOCVD reactor may also need to be considered. This may include adding separate bubbler lines to deliver the Sc and Y MO sources, heating of the MO lines, and increasing the mass flow controller size to deliver adequate MO. The effect of using Sc and Y MOs in the reactor will also need to be evaluated to determine if increased reactor maintenance is necessary.
Accomplishments and changes for Subtask 1.1 – This subtask was accomplished. The three separate MO precursors were purchased and tested for this program. Each of these MO precursors had very low vapor pressure which ultimately limited the amount of Sc or Y that could be incorporated into the GaN films. The reactor modifications that were made for this work are discussed in more detail in Section 4.A.

Subtask 1.2 Add Sc and/or Y to conventional blue and green InGaN based LEDs.
In this subtask, Sc and/or Y will be added directly to InGaN based LEDs to determine if the wavelengths of these blue and green LEDs can be extended to longer wavelengths. These growth runs will provide a quick "proof-of-concept" to validate the entire proposal and possibly uncover potential problems.
Accomplishments and changes for Subtask 1.2 – This subtask was put on hold until Subtask 1.3 could be demonstrated. Unfortunately, in Subtask 1.3 we were not successful in reaching the Sc or Y concentrations required for alloys, therefore research in this Subtask was not completed.

Subtask 1.3 Develop growth and characterization capabilities for ScGaN and YGaN alloys.
After evaluation of the Sc and Y MO sources and reactor modifications, growth of ScGaN and YGaN alloys will commence. Initial growth runs will determine the MO flows necessary to incorporate the Sc and Y. Since our ultimate goal is to use ScGaN and YGaN in multi-quantum wells (MQWs) our focus will be on developing thin layers of these alloys grown on GaN. Growth conditions such as temperature, pressure, and flow rates will be evaluated to increase Sc and Y content. X-ray, RBS, photoluminescence (PL) and possibly secondary ion mass spectroscopy (SIMS) will be used to determine the Sc and Y content in the alloys. During this subtask ScGaN alloys with 20 % Sc content and YGaN with 10% Y content will be demonstrated.
Accomplishments and changes for Subtask 1.3 – This subtask became the major focus of research for the entire first year. Three Sc and Y MO sources were tested under various growth conditions. We were able to successfully incorporate doping level concentrations of Sc and Y into GaN; however we were not able to develop ScGaN or YGaN alloys. More details on the MO precursor's selection, growth details, and results are discussed in Section 4.A.

Subtask 1.4 Demonstrate ScGaN with 50% Sc content and YGaN with 30% Y content.
This subtask is a continuation of subtask 1.3, however the Sc content in the alloy will be increased to 50% and the Y content in the alloy will be increased to 30%. XRD will be used to verify the crystal structure of the ScGaN and YGaN alloys. SIMS may be need on select samples to determine Sc content. PL will be used to determine the wavelength shift.
Accomplishments and changes for Subtask 1.4 – This subtask was put on hold until the completion of Subtask 1.3. Since Subtask 1.3 was not completed before the first year review this Subtask was not completed.

Subtask 1.5 Determine PL wavelength dependence on the Sc and Y contents in alloys.
For this subtask, the growth of the alloys will be varied to improve the crystalline structure. Growth parameters that most influence the crystalline structure of the ScGaN and YGaN alloys will be determined. PL will be used to determine the wavelength shift as a function of Sc and Y content in the alloys. The alloy content will be determined using XRD, RBS, and possibly SIMS if needed. At the conclusion of this subtask, we should know the Sc and Y contents that will be needed to achieve, green, yellow and orange wavelengths.
Accomplishments and changes for Subtask 1.5 – This subtask was put on hold until the completion of Subtask 1.3. Since Subtask 1.3 was not completed before the first year review this Subtask was not completed.

3.3. Tasks developed for no-cost extension and accomplishments

Initially, our work focused on the growth of the ScGaN and YGaN alloys. Before this research, not much work had been conducted on the growth of these alloys using MOCVD. We started by acquiring two yttrium metalorganic precursors and investigated YGaN growth using these precursors which was covered in Task 1 of the proposal. This proved very difficult due to the low vapor pressure of the MOCVD precursors. To date doping level concentrations (~$5x10^{18}$ cm^{-3}) of Y in GaN have been achieved, however to produce useful alloy concentrations of Y in GaN a factor of ~100 increase in the Y concentration is needed. Therefore, achieving Milestones 1.2 through 1.5 (listed below) in Task 1 seemed highly unlikely at this point.

Justification for a no-cost extension

Since YGaN and ScGaN might extend the nitride-LED wavelength to all visible colors, if successful this will be a very novel approach to improving solid state lighting. In this no-cost extension period we will conclude our research on the feasibility of this approach. We expect the remaining work proposed here to take no longer than 9 months and consume the remaining $60K budgeted for the first year of this project. The following research was conducted.

No-Cost Task 1: Additional growth experiments to increase Sc or Y incorporation.

In this task we sought to further explore growth conditions that favor yttrium or scandium incorporation into GaN. The initial stage of the growth research was conducted in a high speed rotating disk reactor (RDR). In August of 2007 the laboratory in which this reactor operated was closed. Growth experiments conducted in this reactor were transitioned to a Veeco D-125 reactor. The separation of the metalorganics from the NH_3 is better in the D-125 reactor than in the RDR as separate injectors are used for the delivery of the metals and NH_3. We thought that if gas-phase parasitic reactions were decreasing the amount of Sc or Y reaching the growth surface, growth in this reactor should help the Sc or Y reach to the growth surface. Also the inlet flange can be heated to decrease metalorganic condensation. Growth conditions such as temperature, pressure, and ammonia flow were varied in the D-125 to investigate if this improves Y or Sc metal incorporation. We focused on growth in N_2 atmospheres because hydrides of yttrium and scandium are surprisingly stable even at temperatures typically used to growth GaN. Formation of the metal hydride either in the gas phase or on the surface is undesirable since it will decrease the metal incorporation into the lattice.

Accomplishments and changes for No-cost Task 1 – The work for this task is reported in Section 4.A under milestone 1.3, since it is a continuation of this milestone to determine if significant quantities of yttrium can be incorporated into GaN. Unfortunately, only doping level quantities of yttrium were ever incorporated in the GaN.

No-Cost Task 2: Purchase and growth using a liquid-Sc precursor.

For this task we purchased a "liquid-like" scandium precursor to determine the extent to which Sc can be incorporated into GaN. Prior to this purchase all of our growth research had been conducted using yttrium precursor. Yttrium was chosen first because it was thought that alloy concentrations would be easier to determine from x-ray diffraction. To date, we have not seen significant yttrium incorporation using the solid yttrium precursor, $(MeCp)_3Y$, while with the liquid yttrium precursor, $(t\text{-}BuCp)_3Y$, we have achieved doping level concentrations as mentioned above. Since ScN is more closely lattice matched to GaN, the Sc might more easily incorporate into the GaN.

Accomplishments and changes for No-cost Task 1 – The work for this task is reported in Section 4.A under milestone 1.3, since it is a continuation of this milestone to see if significant quantities of scandium can be incorporated into GaN using the new more "liquid-like" precursor. Unfortunately, only doping level quantities of scandium were ever incorporated in the GaN.

No-Cost Task 3: Nitridation of sputtered deposited Sc on GaN and GaN grown on ScN.

For the third task we used pulsed laser deposition (PLD) to deposit scandium metals on GaN/sapphire substrates. These metal coated substrates were then put into the MOCVD reactor and exposed to NH_3 and N_2 to form ScN. The purpose of these experiments is two fold and will allow separation of issues associated with the gas phase delivery from issues associated with the surface chemistry. First, having the Sc already deposited on the surface will circumvent difficulties in the gas phase delivery of these low volatility precursors and possible gas phase parasitic depletion of the precursor. Second, converting the Sc metal into nitride on surface would verify that this approach is at least in principle chemically compatible with GaN growth. Brief reports exist in the literature suggesting that N_2 can be used to produce ScN and determining if this was a feasible pathway to form the metal nitrides. If the metal nitrides form using this process, the optical and structural character of these materials will be studied, especially the emission wavelengths.
Accomplishments and changes for No-cost Task 1 –We were able to nitride Sc metal films to form the ScN semiconductor. In addition, we were able to grow coalesced GaN on the ScN films. Research for this result are discussed in Section 4.B.

4. Summary of project activities

4.1. Task 1 summary

Task 1 MOCVD growth of ScGaN and YGaN alloys

Milestone 1.1: Preparation of metalorganic yttrium and scandium precursors.

In June of 2006 a purchase order was made to Epichem LTD for the development of an yttrium based metalorganic (MO) precursor. The precursor that was decided upon was a methylcyclo-pentadienyl ligand or $(Mecp)_3Y$. This precursor was believed to have the highest vapor pressure of any of the surveyed compounds. High vapor pressure of the MO is critical for achieving reasonable growth rates using this compound. Successful growth of p-type GaN is currently accomplished using a similar compound, $(Mecp)_2Mg$.

In September the yttrium precursor was delivered. The proton NMR spectra of $(Mecp)_3Y$ is shown in Fig. 7. The hydrogen shifts shown at 5.9 and 2.0 ppm are consistent with NMR shifts for hydrogen from a cyclopentadienyl ring and methyl group functionality. In the inset the NMR signal for impurities is shown with peak shifts between 2.6 to 3.4 ppm. From this NMR signal, the material does not show any substantial organic impurities; however, there appears to be some oxygen species at < 100 ppm concentration. The oxygen species should have a lower vapor pressure than the $(Mecp)_3Y$ and therefore these oxygenated species will likely remain in the bubbler and not be a significant source of contamination during growth. After we are able to incorporate yttrium into the films secondary ion mass spectroscopy can be performed to determine the level of oxygen contamination.

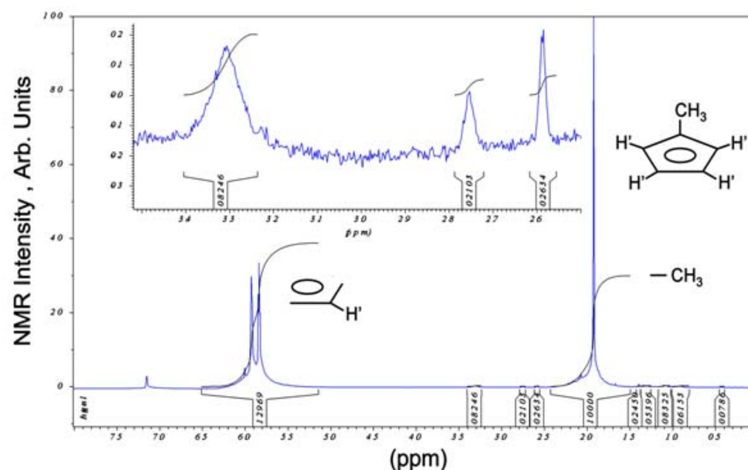

Fig. 7. NMR spectra of the tris-methylcyclopentadienylyttrium, $(Mecp)_3Y$. Hydrogen peaks from the cyclopentadienyl ring (labeled H') occur near 5.9 ppm and hydrogen peaks form the methyl groups (labeled H) occur near 2.0 ppm. From the NMR, the material does not show any organic impurities. There is some oxygen species in <100 ppm concentration.

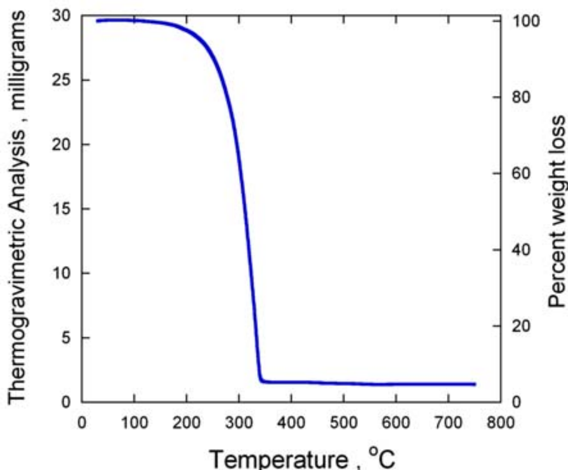

Fig. 8 Thermogravimetric analysis (TGA) of the yttrium precursor. The TGA analysis indicated a very clean material with a low residue of < 5 %, while residue due to the yttrium metal alone would have been around 27 %.

The thermogravimetric analysis (TGA) of the yttrium precursor is shown in Fig. 8. TGA is a measure of the precursor weight loss as the sample is heated and allows for the determination of decomposition temperatures and moisture content. The TGA analysis indicated clean material with a low residue of < 5 %, as the residue due to the yttrium metal alone would have been around 27 %. This analysis suggests that the loss of the precursor is due to vaporization without decomposition and the high sublimation temperature and low residue indicate that the yttrium compound sublimes as an intact molecule.

Separate measurements were also made at Epichem of the $(Mecp)_3Y$ precursor vapor pressure. The vapor pressure is shown in Fig. 9 as a function of temperature. Also shown in Fig. 9 is the vapor pressure vs. temperature of other precursors used in the growth or doping of the group-III nitrides. The vapor pressure data points were measured as the temperature was increased (filled squares) and decreased (open squares) to avoid erroneous readings due to trace solvents in the lower vapor pressure $(Mecp)_3Y$. Note that there is a good correlation for both the increasing and decreasing temperature cases, indicating that in spite of the low vapor pressure, the yttrium compound produces a steady, constant vapor pressure. (Later experimental evidence of this precursor using absorption measurements suggests that the actual vapor pressure of this precursor is much lower than shown in Fig. 9.) At 70 ºC, the vapor pressure of $(Mecp)_3Y$ is 0.42 mmHg, which is low but reasonable for metalorganics with cyclopentadienyl ligands. Note that the vapor pressure of the yttrium and iron dopant, $(cp)_2Fe$, are very similar. At 40 ºC the vapor pressure of the $(Mecp)_3Y$ is a factor of 15,500 lower than trimethylgallium (TMGa), 920 lower than trimethylaluminum (TMAl), and 21 lower than bis-methylcyclopentadienyl-magnesium. While the TMGa and TMAl vapor pressure are high enough to achieve micron per hour growth rates, the magnesium and iron precursors are typically used as dopant sources to achieve doping levels of 10^{17} to 10^{20} cm^{-3} levels in GaN. The impact of the low vapor pressure and possible gas phase pre-reaction will be discussed in detail under Milestone 1.3 of this section.

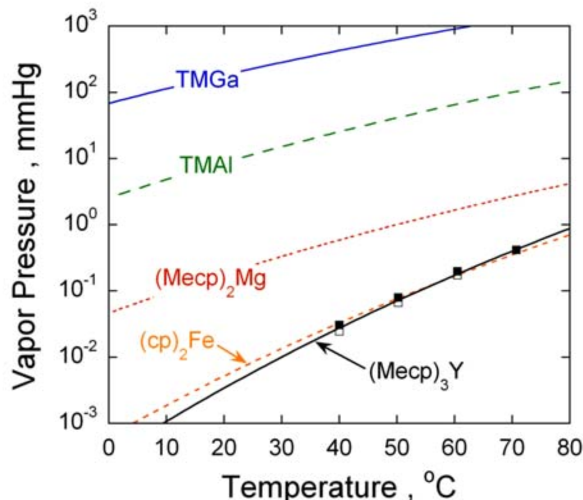

Fig. 9. Vapor pressure curves vs. temperature for the $(Mecp)_3Y$ compound (open and filled squares and black solid line) and other common metalorganic precursors used for growth and doping of the group III nitrides.

In March of 2007 the first yttrium source $(Mecp)_3Y$ was sent back to Epichem for evaluation. The $(MeCp)_3Y$ was returned to Epichem to evaluate the purity, state, and quality of the yttrium source and to determine if the material was still usable. After evaluating the $(MeCp)_3Y$, the scientists at Epichem were unable to find anything wrong with the material in the bubbler. It seems that the major issue with this precursor is that the vapor pressure is too low to be useful even when the bubbler temperature is

run at 80 ºC.

In addition, a second yttrium source was purchased from Epichem. The precursor is tris(n-butylcyclopentadienyl)yttrium or (n-BuCp)$_3$Y. It was believed that this precursor should be a liquid (instead of a solid like (Mecp)$_3$Y) and have a higher vapor pressure compared to (MeCp)$_3$Y. The likelihood of having a higher vapor pressure is due to the n-butyl groups attached to the cyclopentadienyl ring which should produce a greater steric hindrance to solidification. Initial studies show good response in the UV absorbance measurement and it appears that material could be transported out of the bubbler into the growth chamber. Growth tests using this precursor are discussed under Milestone 1.3 in this section. After testing the (n-BuCp)$_3$Y precursor, a similar scandium precursor (tris-n-butylcyclopenta-dienylscandium) was also purchased and put onto the Veeco D-125 reactor. Results with this precursor are also discussed under Milestone 1.3 in this section.

To achieve delivery of the yttrium and scandium sources to the MOCVD chamber substantial modifications were made to the MOCVD reactor including moving the bubbler delivery lines closer to the growth chamber, heat wrapping all of the heater lines to prevent cold spots where the precursor could condense, and installing a UV absorption measurement system both near the bubbler exit and growth chamber entrance. As a result of these modifications, the heating lines can be heated to 80 ºC and have been replaced several times due to failure of the heating tapes. In addition, a UV absorption measurement was installed and was used to verify that the yttrium or scandium precursor is being delivered into the growth chamber. Strong evidence for the delivery of the (t-BuCp)$_3$Y precursor was first observed in April of 2007 after the reactor modifications, keeping in mind that prior to this there was no evidence of (MeCp)$_3$Y delivery to the growth chamber.

Also, during the course of this research our research facilities changed from the compound semiconductor research laboratory (CSRL) to the new Microsystems and Engineering Science Applications (MESA) facility. As a result the custom MOCVD reactor was not moved to the new facility and the research for this program was switched to a Veeco D125 MOCVD reactor. More details on this move and how it affected the research in this program are described in Section 4.C.

Milestone 1.2: Add Sc and/or Y to conventional blue and green InGaN-based LEDs.

Progress on this milestone is delayed until we have achieved Milestone 1.3 and have demonstrated either yttrium or scandium incorporation into GaN.

Milestone 1.3: Achieve ScGaN alloys with 20% Sc (392 nm) and YGaN alloys with 10% Y.

In September of 2006, the (Mecp)$_3$Y bubbler was placed onto the custom rotating disk reactor. Because of the low vapor pressure of the yttrium precursor, reactor modifications were required as previously discussed. Initially, we decided to operate the bubbler at 40 ºC to increase the pre-cursor delivery. This required wrapping and heating all lines that would carry the yttrium to the growth chamber. To further increase the delivery rate of the precursor into the growth chamber, the mass flow controller size was increased to 1000 standard cubic centimeters per minute (sccm). A UV absorption spectrometer was also mounted on the reactor chamber to measure the concentration of yttrium arriving into the chamber by monitoring the UV light absorption by the cyclopentadienyl group.

For the first several growth runs the flow of the TMGa precursor was lowered to achieve a growth rate of 0.2 m/hour and a 1000 sccm flow rate of the (Mecp)$_3$Y precursor was used. The growth was conducted on a GaN template wafer grown previously in the Veeco D-125 MOCVD reactor. Growth was conducted for 1 hour and x-ray analysis of the sample showed no evidence for additional XRD peaks expected for YGaN. In October, 2006, we still had not incorporated a convincing amount of yttrium into GaN yet. X-ray experiments show no observable satellites which would indicate the formation of YGaN alloy. Photoluminescence experiments show

measurable intensity near 372 nm, however it is not clear if this shift in wavelength is due to alloy YGaN formation or due to impurity levels with in the GaN film.

At this time the low vapor pressure of the yttrium precursor was still a major concern. As shown in Fig. 9, the yttrium vapor pressure measured by Epichem at 40 °C is 0.03 millitorr which is equal to the vapor pressure of bis-cyclopentadienyl magnesium at a bubbler temperature at 18 °C. The vapor pressure curve for $(cp)_2Mg$ is not shown in Fig. 9 but is approximately a factor of 5 lower than the vapor pressure curve for $(Mecp)_2Mg$ which is shown in Fig. 9.

Experiments were undertaken to measure the UV absorption of the cyclopentadienyl group by flowing the various precursors into the reactor chamber. To avoid the metalorganics from collecting on cold spots in the reactor gas lines, the gas lines and mass flow controllers were rewrapped with heating tape to ensure uniform heating of all lines to greater than 40 °C. The reactor chamber was heated to 40-50 °C and the chamber screen which provides a laminar flow gas distribution in the reactor was removed. With the yttrium bubbler at 40 °C, the magnesium bubbler at 18 °C, and the trimethylgallium bubbler at -10 °C, each of the metalorganics were flowed into the reactor and the adsorption was monitored at three different wavelengths as shown in Fig. 10. Only hydrogen was flowed along with the metalorganics (i.e. no ammonia) in order to prevent adduct formation and possible precursor condensation. In Fig. 10 the magnesium (blue circles), gallium (red squares), and yttrium (green diamonds) absorption is shown at three different wavelength. Absorption of both the magnesium and gallium precursors is clearly observed, however no absorption is observed for the yttrium precursor; even though the magnesium and yttrium metalorganics should have similar molar flows since they have similar vapor pressures. Possible reasons why no absorption is observed from the yttrium precursor might be due to 1) additional cold spots somewhere along the gas lines, 2) the vapor pressure is much lower than reported by Epichem, or 3) the yttrium precursor is transparent to the wavelengths used for the absorption experiments. A transient UV absorption signal is observed when the yttrium bubbler is first opened after being closed off for a while. This transient UV absorption is probably due to volatile hydrocarbon decomposition product.

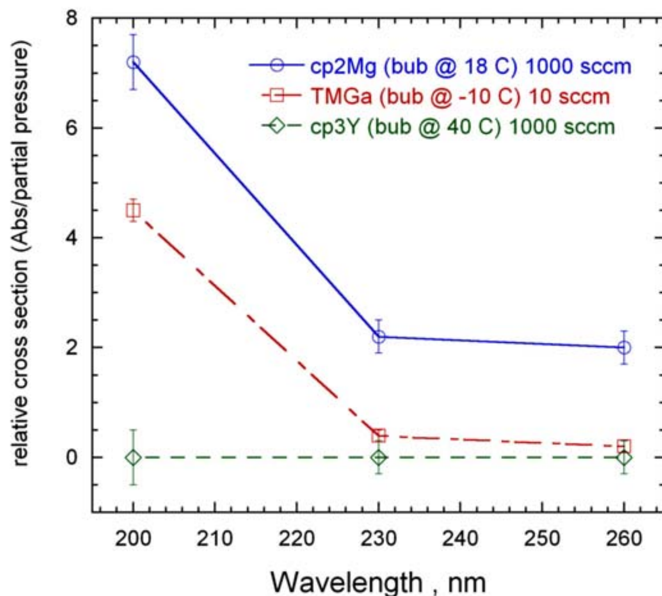

Fig. 10. UV absorption of magnesium (blue circles), gallium (red squares) and yttrium (green diamonds) precursors. The vapor pressures of the magnesium and yttrium precursors are similar and should yield similar adsorption signals.

In November, due to the apparent lack of yttrium precursor flow detected both in the UV absorption measurements and the lack of yttrium incorporation in GaN films, we focused solely on the precursor delivery issue. Several additional modifications were made to the bubbler flow loop, including increasing the stainless steel (SS) tube diameter from $^1/_8$ inch to $^1/_4$ inch, increasing the total flow that can be achieved through the bubbler. Also increasing the tube size should prevent clogging of the bubbler loop if the low volatility precursor condenses on the tube walls. In addition to increasing the tube diameter, the UV absorption spectrometer was moved from being close to the reactor chamber to being closer to the bubbler. After completing the new welded SS pieces and leak checking the new bubbler delivery system, UV absorption measurements were conducted and a positive indication of the yttrium precursor flow was detected as shown in Fig. 11.

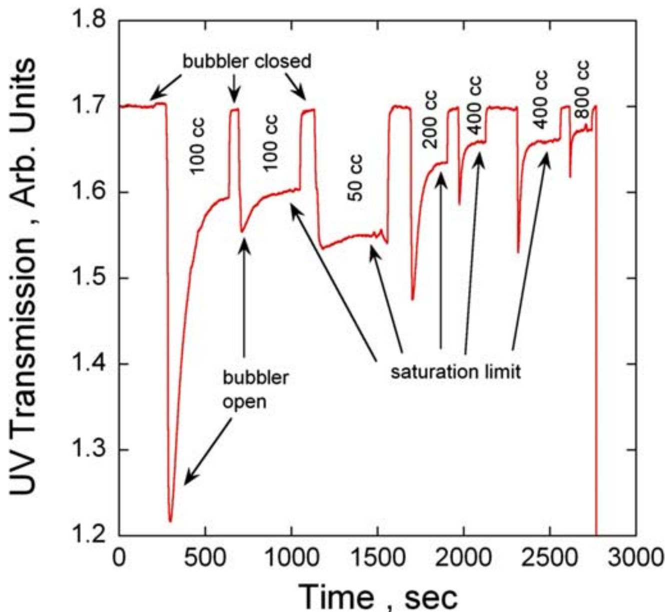

Fig. 11. The UV transmission through the UV cell is plotted as a function of time for different bubbler flow rate conditions with the bubbler both open and closed. The bubbler loop pressure was held at 600 torr and bubbler temperature at 50.7 °C. Note that once the bubbler is first opened there is a larger decrease in the UV transmission due to an increase in the absorption from the cyclopentadienyl groups flowing through the UV cell. Flow conditions ranged from 50 to 800 sccm.

The UV transmission through the UV cell shown in Fig. 11 is shown for different carrier gas flow conditions through the bubbler. A decrease in the transmission corresponds to an increase in the absorption, providing a positive indication for the presence of the precursor in the carrier flow. *This was a major breakthrough for this project, because previous attempts to detect this precursor in the gas phase had all failed.* We also observed several non-traditional behaviors of the yttrium bubbler which will greatly help us in future growth experiments with this precursor.

The first behavior which had been previously indicated in the UV absorption was the presence of a large transient absorption once the bubbler is opened for the first time or after it has been closed temporarily. This is most dramatically observed by the large decrease in the transmission once the bubbler is opened for the first time near 300 seconds. Note further that after the bubbler is closed and then opened there is a sharp decrease in the transmission, the degree of which depends on how long the bubbler was previously closed. This can be most clearly observed for the 400 sccm flow rates between 2000 and 2500 seconds. For the first 400 sccm flow measurement the bubbler was closed for 1 minute prior to opening while for the second 400 cc flow measurement the bubbler was closed for 3 minutes prior to opening. Note that the transmission decreases to a greater extent for the 3 minute closing compared to the 1 minute closing. This result indicates that the precursor is not fully saturated in the gas phase of the bubbler and suggests that there is a large kinetic barrier to evaporation for the precursor thus resulting in a lower concentration of the precursor in the gas phase with carrier gas flow time.

This gas phase depletion of the precursor limiting the precursor transportation is also supported by the unusual decrease in the gas phase concentration of the precursor as the carrier gas flow rate increases. This is shown in Fig. 11 by the saturation limit that is reached after the bubbler has been opened for a length of time. The saturation limit is indicated in Fig. 11. Note that the transmission level is higher (i.e. lower absorption which results from a lower precursor concentration in the gas phase) as the carrier gas flow increases, indicating that the precursor concentration decreases as the carrier gas flow increases. Normally, for bubblers with higher volatility precursors, the precursor concentration in the gas phase is independent of the carrier gas flow rate through the bubbler. However, because of the kinetically inhibited volatility of the yttrium precursor, the gas phase concentration can not be replenished fast enough and the precursor concentration in the gas phase decreases with increasing carrier gas flow rate.

In December, based on the previous UV absorption measurements the molar flow rate of the yttrium precursor is shown in Fig. 12 as a function of the flow rate through the bubbler. For this plot the molar flow rate through the bubbler is related to the precursor gas phase concentration

time the carrier gas flow rate. If the yttrium precursor completely saturated the gas phase then the molar flow rate would be constant which should result in a linear relationship between the precursor concentration and the carrier flow rate. This ideal precursor behavior for the molar flow rate into the MOCVD growth chamber would result in the linear relationship shown in Fig. 12 by the blue line. However, if the precursor does not completely saturate the gas phase, then a sub-linear dependence of the molar flow rate on the carrier flow rate is expected as shown by the red line in Fig. 12. Unfortunately this second behavior is what we observed for the yttrium precursor.

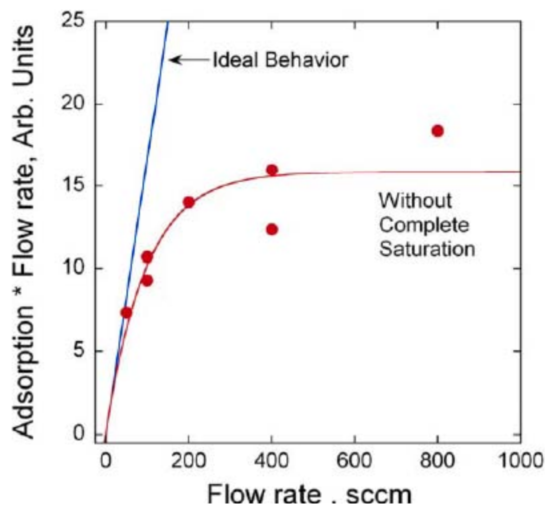

Fig. 12. Using the UV transmission data, the product of the UV absorption and the flow rate through the bubbler is plotted vs. the flow rate. This product should be proportional to the molar flow rate out of the bubbler. If the precursor saturates the gas phase then the ideal behavior is observed and the molar flow rate depends linearly on the flow rate through the bubbler. However if the precursor does not saturate the vapor phase then the molar flow rate will be sub-linear as shown by the data in red.

One way to increase the vapor phase saturation is to increase the bubbler temperature which will increase the sublimation rate of the precursor. The bubbler heater and lines were improved so that a bubbler temperature of 80 ºC could be achieved. Using this higher bubbler temperature, YGaN films were again attempted using a flow rate of 200 sccm through the bubbler.

Photoluminescence (PL) measurements of the YGaN film on top of GaN were similar in band edge wavelength position however the intensity was decreased, indicating a possible incorporation of only dopant level amounts of yttrium. Secondary ion mass spectroscopy (SIMS) was also conducted on an older YGaN sample to check for gross impurity contamination and yttrium incorporation. Yttrium was only found at background levels indicating no incorporation of yttrium for this sample.

In January of 2007, we continued experiments to determine if yttrium could be deposited in the MOCVD reactor. We attempted to deposit yttrium (without ammonia) on a silicon wafer, but the analysis of the film did not show any yttrium deposition.

We also tried methods to increase the precursor surface area within the bubbler, in an attempt to improve bubbler efficiency. The first method tried, which is commonly used on solid sources, was to take the bubbler off the reactor and hit it multiple times with a plastic hammer. We also verified that the bubbler contained at least 23 grams of precursor (out of the original 25 grams), so gross depletion of the source cannot be the problem with delivery. After applying the "hammer method" the bubbler was reinstalled on the reactor and no change was observed in the behavior of the yttrium bubbler. Again the bubbler was taken off the reactor and placed in an ultrasonic bath in an attempt to break up the precursor, followed by more treatment with the hammer. After reinstallation on the reactor there was again no improvement in yttrium concentration. In fact, the general long-term decline in yttrium concentration continued.

In February of 2007 we purchased another yttrium source from Epichem. This bubbler is tris(n-butylcyclopentadienyl)yttrium or $(n\text{-}BuCp)_3Y$. The difference between this precursor and the one previously used is that instead of a methyl group substituted on the cyclopentadienyl group an n-butyl group is used. The $(n\text{-}BuCp)_3Y$ precursor should be a liquid and have a higher vapor pressure compared to $(MeCp)_3Y$. The $(n\text{-}BuCp)_3Y$ precursor will be used without purification to see if we can transport it to the reactor. Also, for best delivery of the $(n\text{-}BuCp)_3Y$ bubbler it may need to be heated to 110 °C, which may require some modification to bubbler heating method.

In April of 2007 the new yttrium bubbler was placed on our custom MOCVD reactor. In addition, we rewrapped the entire yttrium gas line from the bubbler to the growth chamber with new heating tape. The entire bubbler line and bubbler can now be heated to ~80 ºC. Rewrapping the lines also corrected one colder spot that may have negatively affected previous work by trapping some of the yttrium precursor. After these modifications, the UV absorbance measurements indicated presence of precursor exiting the bubbler and entering the growth chamber. The observation of a reproducible UV absorbance signal provides us with some confidence that the yttrium precursor is finally making it into the growth chamber. After observing the UV absorbance signal, approximately 6 growth runs were conducted. For these growth runs growth parameters such as the bubbler temperature, growth temperature, carrier gas (N_2 or H_2) were varied to produce growth of either the YGaN alloy or the binary compound YN. All films were deposited on well characterized GaN templates on sapphire.

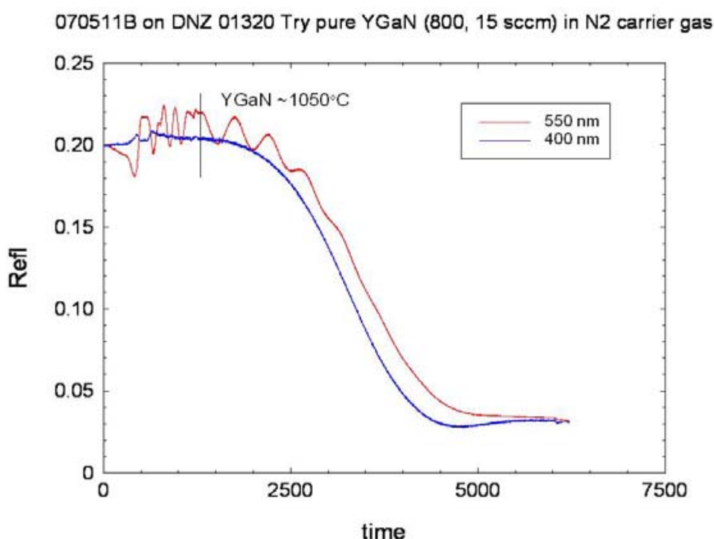

Fig. 13. Optical reflectance waveform at 550 nm (red) and 400 nm (blue) for an attempt at YGaN alloy growth. The decrease in the optical reflectance signal is due to surface roughening which is induced via the introduction of the yttrium precursor.

In Fig. 13 is shown an optical reflectance waveform at 550 nm for an attempt at YGaN growth at 1050 ºC in only N_2 carrier gas. Typically, GaN and most of the YGaN growth attempts have been conducted in H_2 carrier gas. One reason the growth might be more successful in N_2 carrier gas would be to avoid gas phase pre-reactions. We also thought H_2 might be etching the yttrium or preventing incorporation into the film. However, the decrease in the optical reflectance signal after the yttrium is introduced into the growth chamber looks similar to growth experiments in H_2 carrier gas. The induced roughening is most likely due to either yttrium or other impurity causing a re-nucleation of GaN growth on top of the original GaN template and is evidence that the introduction of the yttrium precursor is causing some effect on the growth. After roughening, in some cases the films would partially recover to yield reflectance values of 0.12-0.14 (specular GaN reflectance = 0.20).

The surface roughening observed in the optical reflectance is also evident in Nomarski phase contrast microscope images shown in Fig. 14. The hexagonal symmetry observed in Fig. 14 is expected of wurtzite material. Also observed in Fig. 14(b) and (c) is additional re-nucleation on the vertices on some of the hexagonal platelets is evident. So far x-ray diffraction of this sample and other growths in this series have not shown a distinct diffraction peak for the presence of YGaN, nor has a

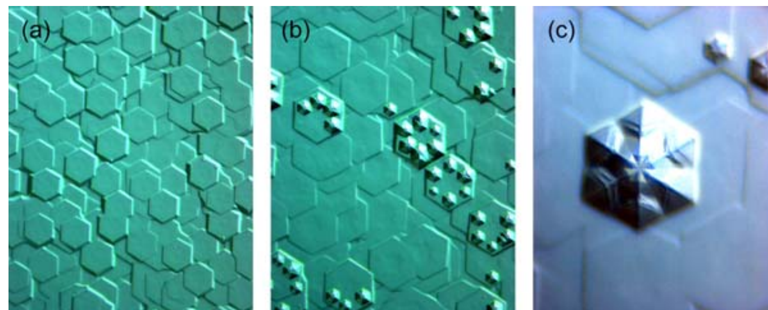

Fig. 14. Nomarski phase contrast images of the roughened film produced when the yttrium precursor is introduced during GaN growth. The objective magnification for each of the images is (a) x50, (b), x50, and (c) x100. The hexagonal symmetry is expected of wurtzite material and may occur due to yttrium or impurity induced re-nucleation on the original GaN surface.

distinct shift observed in the photoluminescence that can be uniquely attributed to the YGaN alloy.

To verify that some yttrium was incorporated into the GaN, SIMS measurements were performed and the SIMS depth profiles are shown in Fig. 15. The SIMS concentrations of yttrium (orange open circles) and silicon (open red squares) in GaN are plotted in Fig. 15 as a function of film thickness. Also plotted are the common atmospheric impurities hydrogen, carbon, and oxygen. The GaN substrate films were silicon doped to better delineate the interface between the substrate and the yttrium doped GaN film. In Fig. 15, the silicon level decreases approximately 1.5 m below the surface indicating that ~ 1.5 m of yttrium doped GaN is grown on top. Note the gradual increase in the yttrium concentration from the background level at ~ 10^{14} cm^{-3} to a concentration of $5.3x10^{18}$ cm^{-3} near the surface. At the surface the yttrium concentration as well as the other impurity concentration increases due to a change in the SIMS matrix ionization probability. This increase is typically ignored in any quantitative analysis of the bulk concentrations. Also, instead of a sharp increase in the yttrium concentration it takes almost 0.5 μm to reach concentrations in the 10^{18} cm^{-3} indicating a possible delayed turn on effect which is also commonly observed during Mg doping of GaN. Another possible reason for the delay in the yttrium reaching a steady concentration might be due to the increased surface roughness. (Increased surface roughness can cause the appearance of gradual changes in elemental concentrations due to the different depths to be sputtered during the SIMS analysis.) Finally, although the liquid yttrium precursor was used without purification, the yttrium doped GaN layer does not show higher than normal concentrations of oxygen and carbon, indicating that the yttrium precursor impurities should not be a major concern, yet.

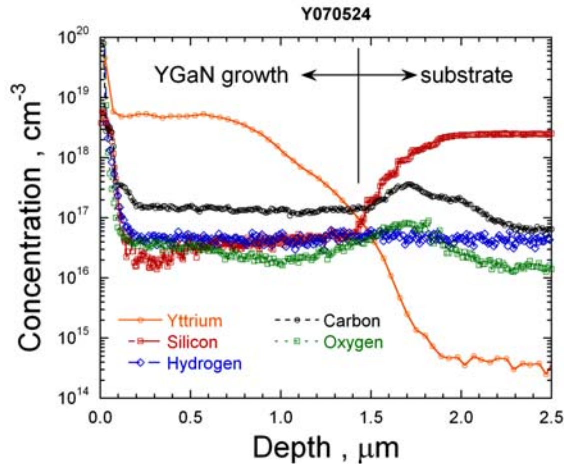

Fig. 15. Secondary ion mass spectroscopy (SIMS) of yttrium (orange open circles) incorporation in GaN. The GaN substrate was silicon (red open squares) doped so that the interface between the GaN substrate and the yttrium doped region could be clearly discerned. The yttrium concentration reaches a level of $5.3x10^{18}$ cm^{-3} for a thickness of ~0.6 m.

From the SIMS data shown in Fig. 15 we have for the first time shown that yttrium can be incorporated into GaN, regrettably however, as mentioned above, we are still far below achieving alloy quantities of yttrium in GaN. With the density of GaN of $8.79x10^{22}$ atoms/cm^3, we need to increase the yttrium concentration 166 times in order to achieve a 1% YGaN alloy. Since the injection scheme is more direct in the Veeco D-125 we hoped to get more efficient injection of the yttrium precursor in the growth chamber.

After the Veeco D-125 MOCVD reactor was moved to the new MESA facility and passed Safety Levels 1 and 2, growth runs using the $(n\text{-}BuCp)_3Y$ source liquid yttrium precursor were done. Several additional growth runs were conducted however only doping level quantities of yttrium were obtained.

After testing the liquid yttrium precursor, the new liquid scandium precursor (tris-n-butyl-cyclopenta-dienylscandium) was put onto the MOCVD reactor. A growth run with the scandium precursor was conducted with the bubbler temperature at 65 °C and the growth chamber pressure at 50 torr. The scandium was introduced into the chamber while GaN was growing at a slower growth rate, after which the scandium precursor was shut off and the sample capped with GaN. Unlike the yttrium doped sample, no significant decrease in the optical reflectance signal was noticed. Scandium incorporation in GaN was verified using SIMS measurements with the results

shown in Fig. 16. For this SIMS measurement, the ScGaN film was grown on a GaN template and capped with GaN to reduce the SIMS surface matrix effect which tends to increase the concentrations of most elements near the surface. Near the surface labeled by (1) the scandium concentration is near the detection limit of $1x10^{14}$ cm^{-3} and then increases when the sputtering depth reaches the Sc doped GaN region of the film which is labeled by (2) in Fig. 1. Unfortunately, a concentration of only $1x10^{17}$ cm^{-3} was detected for scandium which is similar to the previous result with yttrium where only doping level concentrations were incorporated into the GaN. This concentration of scandium is many orders of magnitude lower than what is needed to form ScGaN alloys.

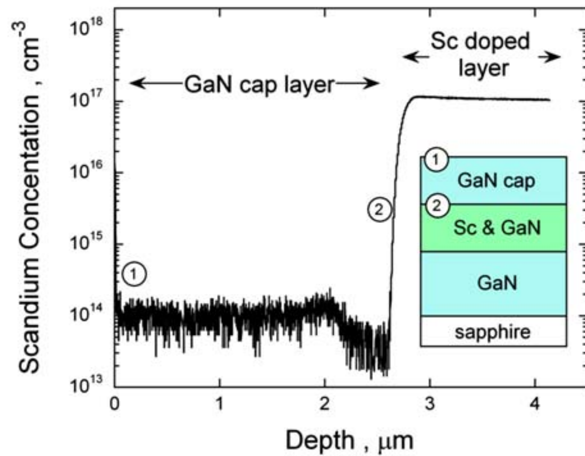

Fig. 16. Secondary ion mass spectroscopy (SIMS) depth profile for the element scandium of sample grown using the liquid scandium precursor. On top of a GaN template scandium was introduced at a slower GaN growth rate to increase the level of scandium in the GaN. A GaN capping was grown on top of the scandium doped GaN layer to eliminate SIMS surface effects on the scandium concentration measurement.

Two additional samples have been grown with the liquid scandium precursor, one where only the scandium metal was turned on with flowing ammonia and one where the GaN growth rate was reduced by a factor of 10 compared to the GaN growth rate shown in Fig. 16. Both of these samples were capped with GaN similar to the sample shown in Fig. 16. SIMS profiles were conducted on both the samples and scandium at a level of $1.5x10^{17}$ cm^{-3} was detected.

Unfortunately, the scandium incorporation into GaN was not much above doping level quantities. As a result the major focus of the no-cost extension was shifted to nitridation of deposited scandium films on GaN. This research is discussed in Section 4.B.

Milestone 1.4 Achieve ScGaN alloys with 50% Sc and YGaN alloys with 30% Y.

This milestone was not achieved because only dopant levels of Sc and Y were obtained in Milestone 1.3.

Milestone 1.5 Determine PL wavelength dependence on Sc and Y contents in alloys. Determine target Sc and Y concentration needed in alloys to achieve green, yellow, and orange LEDs.

This milestone was not achieved because only dopant levels of Sc and Y were obtained in Milestone 1.3.

4.2. Tasks performed under the no-cost extension

Task 1, "additional growth experiments to increase Sc or Y incorporation" and task 2 "purchase and growth using a liquid-Sc precursor" were previously discussed in Section 4.A. Here we discuss Task 3 from the no-cost extension "Nitridation of sputtered deposited Sc on GaN and GaN grown on ScN".

Task 3 - Nitridation of sputtered deposited Sc on GaN and GaN grown on ScN

Initially, the work focused on three areas: deposition of Sc-metal films on GaN/sapphire templates, subsequent nitridation of these films to form ScN, and characterization of the resulting Sc and ScN thin-film materials.

Initially, 36 Sc-metal films with thicknesses of 3, 6, 9, 12, and 50 nm were deposited onto GaN/sapphire templates using pulsed-laser deposition (PLD). The Sc depositions were carried out with the samples at room temperature in a vacuum in the low 10^{-6} Torr range. A time-of-flight collimation system was used during the PLD process to select Sc-metal vapor from the laser-ablation plume, thereby preventing Sc-metal droplets from depositing onto the samples. The GaN/sapphire templates were 4 μm thick GaN films deposited on c-plane sapphire by metal-organic chemical vapor deposition (MOCVD). To accommodate sample-size limitations imposed by the design of the PLD system, the 2-inch-diameter GaN/sapphire template wafers were diced into quarter-wafer pieces for these experiments.

Following deposition of the Sc metal films, individual quarter-wafer samples were returned to our MOCVD reactor and nitrided for 30 minutes at 1050 °C in an ambient of NH_3/H_2 or NH_3/N_2. For the first three NH_3 exposures the nitrided Sc films were all 9-nm thick. The ambient pressure during our first NH_3/H_2 nitridation was 200 Torr; the pressures during two subsequent nitridations in NH_3/N_2 were reduced to 50 Torr and then 20 Torr. The switch from H_2 to N_2 carrier gas and the use of these lower reactor pressures were done to improve the lateral uniformity and planarity of the nitrided surface.

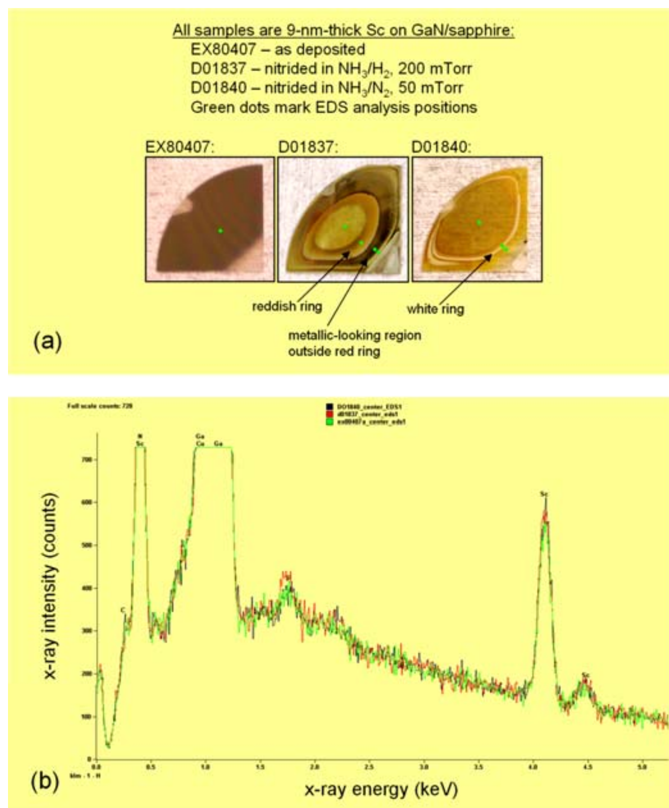

Fig. 17. (a) Photographs of Sc-metal films deposited on GaN/sapphire quarter-wafer templates; the photos are taken before and after nitridation in NH3 at 1050 °C. (b) SEM/EDS spectra taken near the center of each of the three samples. The Sc Ka peaks near 4.09 keV have similar intensities before and after nitridation indicating that the samples do not lose Sc during nitridation.

Following nitridation, the samples were photographed and then characterized by scanning electron microscopy in combination with energy-dispersive x-ray spectroscopy (SEM/EDS). Photographs in Fig. 17(a) show an as-deposited Sc-metal film (on left), the film nitrided in NH_3/H_2 at 200 torr (at center), and the film nitrided in NH_3/N_2 at 50 torr. Upon nitridation, the films change color from opaque grey to translucent orange-brown. The distinct change in opacity suggests either loss of the Sc metal from the surface or conversion to a transparent semiconductor. Figure 17(b) shows EDS spectra taken at the center of each sample. Using similar EDS analysis conditions, we find nearly equal intensities for the Sc K_α x-ray peaks seen near 4.09 keV for each sample, leading us to conclude that the Sc remains present in all cases. Since Sc is not lost from the samples, we infer that nitridization of the metal to produce semiconducting ScN has indeed occurred. Finally, comparing the appearance of the two nitrided samples, we note that lowering the nitridation pressure does improve sample uniformity. Yet further improvement is seen for nitridation at 20 Torr in a NH_3/N_2 gas mixture, but with reductions in the nitridation time and temperature.

Comparing recent 1050 °C nitridations conducted at 20 torr for 15 or 30 minutes to previous nitridations conducted at 50 or 200 torr for 30 minutes reveals a trend where both increased times and increased pressures lead to an increasingly distinct ring-like pattern at the periphery of the sample, accompanied by a diffuse, slightly grey-colored tinting in the center region of the sample. The diffuse grey may be Ga metal produced by decomposition of the underlying GaN during the nitridation anneal. To test for decomposition, the 15-minute-long nitridation was repeated at a reduced temperature of 950 °C, which should reduce any GaN decomposition. This sample actually ended up somewhat more grey in color, which is opposite of expectations if GaN decomposition is the sole cause of the diffuse-grey tinting of the ScN films. Because the lower 950 °C temperature also reduces the nitridation rate such that Sc metal may remain in the film nitrided at lower temperature, it may be that there are two competing effects leading to observed changes in the grey sample appearance.

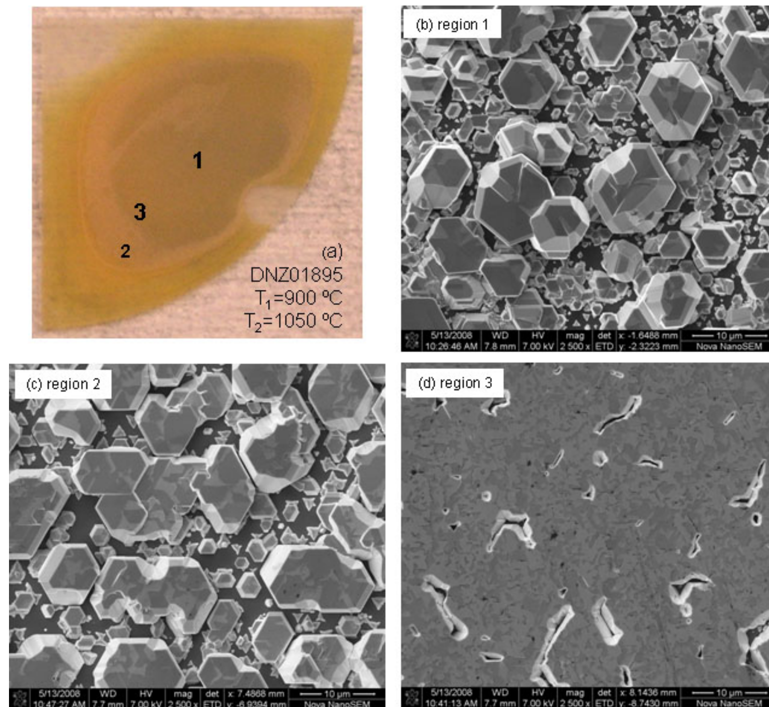

Fig. 18. (a) Sample photograph and (b-d) SEM images of GaN grown on 16-nm-thick ScN layers on top standard GaN/sapphire templates using a two-step nucleation and growth procedure. GaN is nucleated at temperature T_1=900 °C for 15 minutes, and then temperature is ramped to T_2=1050 °C for an additional 60 minutes of growth. Numbered labels in panel (a) indicate the positions where SEM images were taken.

Following these nitridations, selected samples were used for GaN regrowth to see if ScN can help to reduce GaN dislocation density. At first, a single-step approach was used where the GaN growth proceeded at a normal high temperature near 1050 °C. Further GaN growths used a two-step approach where initial nucleation took place for 15 minutes at reduced temperatures of 950 °C, 900 °C, and 850 °C followed by continued growth at 1050 ºC for 60 minutes.

Fig. 18 shows SEM images of the resulting surface morphology for a sample where the first 15 min. was grown at 900 ºC followed by 1 hour at 1050 ºC. Note that the SEM images show rough morphologies comprised of partially oriented crystallites that range in width from < 1 µm up to ~10 µm. Partial coalescence of the GaN film on the ScN layer is observed near region 3 (image (d)) of the sample. The degree of GaN crystallite orientation varies with nucleation temperature, with the lower temperature sample showing the most highly oriented domains (Fig. 2c). The degree of orientation also varied with lateral position for each sample and these lateral variations may arise from lateral variations in the thickness and structure of the ScN layer, or from non-uniform GaN growth conditions on the ScN layer. Laterally uniform, highly oriented nuclei are needed to obtain low threading-dislocation densities in the regrown, coalesced GaN.

Further SEM studies of the GaN regrowths continued to show poor coalescence of the GaN on ScN, but we have now identified a possible reason for the difficultly in obtaining full coalescence. We believe that GaN coalescence is inhibited on the ScN due to a lack of nucleation sites necessary for GaN grain growth. This viewpoint was reached after GaN regrowth experiments on

9-nm-thick Sc film on an AlN/sapphire template. Near the center of the regrowth experiment we observed poor grain orientation, dense parasitic nucleation, and little lateral growth of GaN – roughly similar to previous attempts at higher nucleation temperatures. However, at the wafer edge, we observed something completely different. The film is partially coalesced and has a fractal-like triangular pattern. The pattern results from previous fracture of the underlying AlN due to tensile stress concentrations at the wafer edge. The fracture grooves serve as efficient nucleation sites for GaN regrowth, and nucleation is followed by epitaxial lateral overgrowth where GaN stripes of uniform thickness grow laterally out of each fracture groove.

From the growth experiments on the Sc/AlN/sapphire, our working hypothesis was that our Sc metal films deposited by PLD have few or no pinholes because they are too thick (6-15 nm for GaN regrowths to date), while those previously reported by Moram et al [APL **91**, 152101 (2007)] may have had many pinholes. Their Sc metal films were deposited by magnetron sputtering, which may lead to a different, more-porous film structure than observed for our PLD Sc films. To test our hypothesis we performed Sc nitridations and GaN regrowths using our thinnest available 3-nm-thick Sc films, which should thin enough to have enough pinholes to efficiently nucleate GaN during regrowth.

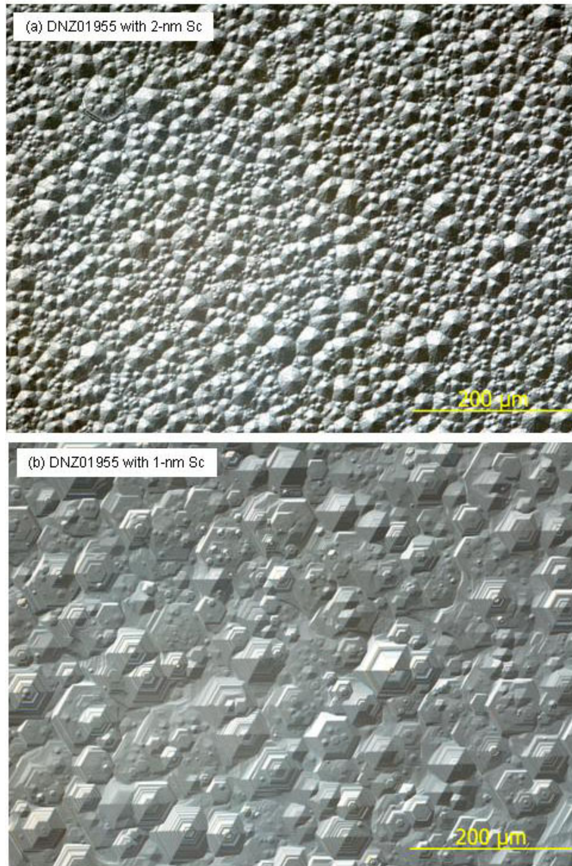

Fig. 19. Nomarski optical microscopy of the growth surface of coalesced, 2-µm-thick GaN regrown on thin ScN interlayers (200X magnification via eyepiece). Labeled Sc-film thicknesses are for the as-deposited metal film prior to nitridation and regrowth.

To examine our hypothesis further, we performed AFM of one of our 9-nm-thick Sc metal films. The rms surface roughness of the starting AlN template was 0.11 nm, and the roughness of the subsequent PLD-deposited Sc was only 0.27 nm. Since this roughness is much less than the 9-nm film thickness, we infer that these films will have very few pinholes or perforations due to random thickness fluctuations, which supports our hypothesis.

To obtain Sc films containing a higher density of random pinholes, thinner Sc-metal films were fabricated with as-deposited thicknesses ranging from 1 to 2 nm. These thinner Sc films were deposited on thinner GaN templates (~1-um thick) with a much higher threading-dislocation density (~1.1×10^{10} cm^{-2}). This change in templates makes it easier for us to detect improvements in any thick GaN overlayers regrown on the ScN.

SEM and Nomarski optical microscopy studies of our latest GaN regrowths on ScN now show that GaN regrowths on very thin ScN films do coalesce to produce continuous films. This result verifies our hypothesis, where we contended that thinner, more porous ScN films are needed in order to increase the number of GaN nucleation sites, which are thought to result from pinholes in the ScN film. While the most recent GaN regrowths have coalesced, the regrown GaN surface remains non-specular indicating that the coalesced surface is rough on optical length scales. Nomarski microscopy reveals textured a surface structure dominated by either hexagonal or dome-shaped domains (Fig. 19). Yet further study and optimization of GaN nucleation on ScN is required to obtain a suitably smooth surface during GaN regrowth.

We also performed a separate photoluminescence (PL) survey of several ScN films previously prepared from 9-nm-thick Sc films on GaN/sapphire. The PL was measured at room temperature using an Accent RPM 2000 PL mapper delivering 325-nm excitation from a HeCd laser. No optical emission other than that expected for GaN was detected. The lack of ScN emission could be due to the polycrystalline structure of the ScN layer that likely contains numerous non-radiative centers that quench optical emission or the ScN might not be a direct bandgap semiconductor. Further XRD and nitridation studies using much thicker Sc layers are needed to verify the polycrystalline character of our ScN layers; 50-nm-thick Sc layers have already been deposited and are available for future studies.

Throughout the no-cost extension, 50 Sc-metal films were deposited on GaN, AlN, or AlGaN templates on sapphire. Of these films, 24 have been reactor annealed to produce thin ScN films, and 22 of these have undergone subsequent GaN regrowth in order to examine GaN nucleation and growth on the ScN surface. Substantial progress was made toward GaN regrowth on the ScN films. Since this project has ended as of June 30, 2008, any further experiments on ScN layers, particularly studies of their use for dislocation reduction in GaN and strain-relaxed InGaN, will be conducted via our ongoing Project #M6642865, *Innovative Strain-Engineered InGaN Materials for High-Efficiency Deep-Green Light Emission*.

4.3. Work performed in support of all Tasks

(Decommissioning Custom MOCVD reactor, moving Veeco D-125 MOCVD reactor to new MESA facility, and moving the research to the Veeco D-125 Reactor in the new MESA facility).

In August 2007, we were required to shut down the custom MOCVD reactor where the research for this program was being conducted. In December of 2007, this research was moved to a Veeco D-120 MOCVD reactor which had been moved to the new Microsystems and Engineering Sciences Applications (MESA) facility.

5. Summary of project activities

In this research program, we attempted to grow ScGaN and YGaN alloys using MOCVD to replace the InGaN active regions in nitride-based LED structures. The major problem we encountered was the low vapor pressure of the scandium and yttrium metalorganic precursors (MOs). The low vapor pressure of the Y and Sc precursors meant that we were unable to deliver adequate MO to the growth chamber to grow ScGaN and YGaN alloys. We were able to achieve doping level concentrations of both Y and Sc into GaN at levels up to $5x10^{18}$ cm^{-3}. These doping level quantities are ~100 times lower than the levels needed to achieve 1% alloy concentrations of these metals. Future MOCVD growth of ScGaN or YGaN will likely require substantial reactor modification, including the development of specialized MO injectors to deliver the low vapor pressure precursor directly to the growth region, reactor designs or growth conditions that reduce gas-phase parasitic particulate formation, and ways to prevent gross changes in the growth morphology as shown in Fig. 14.

During the no-cost extension, we focused on nitriding deposited Sc films on GaN. We successfully nitrided the metallic Sc to form ScN. In addition, we were able to coalesce GaN films on the thin ScN films. The ScN films, however, did not show any appreciable luminescence, possibly due to poor crystal quality or the lack of a direct bandgap transition in the material.

6. References

[1]. A.R. Smith, H. A. H. AL-Brithen, D. C. Ingram, and D. Gall, J. Appl. Phys. 90, 1809 (2001).

[2]. C. Stampfl, W. Mannstadt, R. Asahi, and A. J. Freeman, Phys. Rev. B 63, 155106 (2001).

[3]. J. Wu, W. Walukiewicz, K. M. Yu, J. W. Ager III , E. E. Haller, H. Lu, and W. J. Schaff, Appl. Phys. Lett. **80**, 4741 (2002).

[4]. T. Mukai, M. Yamada, and S. Nakamura, Jpn. J. Appl. Phys. 38, 3976 (1999).

[5]. D. D. Koleske, A. J. Fischer, A. A. Allerman, C. C. Mitchell, K. C. Cross, S. R. Kurtz, J. J. Figiel, K. W. Fullmer, and W. G. Breiland, Appl. Phys. Lett. 81, 1940 (2002).

[6]. C. Wetzel and T. Detchprohm, MRS Internet J. Nitride Semicond. Res. **10**, 2(2005).

[7]. T. M. Smeeton, M. J. Kappers, J. S. Barnard, M. E. Vickers, and C. J. Humphreys, Phys. Stat. Sol. (b) 240, 297 (2003).

[8]. Y.T. Moon, D.J. Eim, K.M. Song, C.J. Choi, S.H. Han, T.Y. Seong and S.J. Park, J. Appl. Phys. 89, 6514 (2001).

[9]. Y.-H. Cho, S. K. Lee, H. S. Kwack, J. Y. Kim, K. S. Lim, H. M. Kim, T. W. Kang, S. N. Lee, M. S. Seon, O. H. Nam, and Y. J. Park, Appl. Phys. Lett. 83, 2578 (2003).

[10]. T.P. Das and M. Pomerantz, Phys. Rev. 123, 2070 (1961).

[11]. I. Ho and G. B. Stringfellow, Appl. Phys. Lett. 69, 2701 (1996).

[12]. M. D. McCluskey, L. T. Romano, B. S. Krusor, N. M. Johnson, T. Suski and J. Jun, Appl. Phys. Lett. 73, 1281 (1998).

[13]. D.D. Koleske, A.E. Wickenden, R.L. Henry, W.J. Desisto, and R.J. Gorman, J. Appl. Phys. 84, 1998 (1998).

[14]. O. Ambacher, M.S. Brandt, r. Dimitrov, T. Metzger, M. Stutzmann, R.A. Fischer, A. Miehr, A. Bergmaier, G. Dollinger, J. Vac. Sci. Technol. B 14 (1996) 3532.

[15]. D.D. Koleske, A.E. Wickenden, R.L. Henry, M.E. Twigg, J. Cryst. Growth 242, 55 (2002).

[16]. P. B. Klein, S. C. Binari, K. Ikossi, A. E. Wickenden, D. D. Koleske, and R. L. Henry, Appl. Phys. Lett. 79, 3527 (2001).

[17]. C.H. Seager, D.R. Tallant, J. Yu, W. Gotz, J. of Luminescence 106, 115 (2004).

[18]. S. M. Myers, A. F. Wright, G. A. Petersen, W. R. Wampler, C. H. Seager, M. H. Crawford, and J. Han, J. Appl. Phys. **89**, 3195 (2001).

[19]. Z. Gu, J. H. Edgar, J. Pomeroy, M. Kuball, D. W. Coffey, J. Mat Sci.: Mat. Electron. 15, 555 (2004).

[20]. Properties of Group III Nitrides, edited by J. H. Edgar, Electronic Materials Information Service (EMIS) Datareviews Series (Institution of Electrical Engineers, London, 1994).

[21]. Pearson's handbook of crystallographic data for intermetallic phases, edited by P. Villars and L. D. Calvert (American Society for Metals, Metals Park, Ohio, 1985)

[22]. Vegard's Law is assumed, L. Vegard, Z. Phys. **5**, 17 (1921).

[23]. L. Mancera, J. A. Rodríguez, and N. Takeuchi, phys. stat. sol. (b) 241, No. 10, 2424–2428 (2004).

[24]. J. P. Dismukes and T. D. Moustakas, Proceedings of the III–V Nitride Materials and Processes Symposium, ECS, 96-11, 111(1996).

[25]. M.E. Little and M.E. Kordesch, Appl. Phys. Lett. 78, (2001).

[26]. CRC Handbook of Chemistry and Physics, 85th Edition, 2004-2005 (CRC Press, LLC, Cleveland, 2004).

[27]. A.A. Allerman, M.H. Crawford, A.J. Fischer, K.H.A. Bogart, S.R. Lee, D.M. Follstaedt, P.P. Provencio, D.D. Koleske, J. Crystal Growth 272 (2004) 227–241.

[28]. J. Nord, K. Albe, P. Erhart and K. Nordlund, J. Phys.: Condens. Matter 15, 5649 (2003).

[29]. J. R. Creighton, G. T. Wang, W. G. Breiland, M. E. Coltrin, J. Crystal Growth 261, 204 (2004).

[30]. M.E. Little and M.E. Kordesch, Appl. Phys. Lett. 78, (2001).

[31]. D. Gall, I. Petrov, N. Hellgren, L. Hultman, J. E. Sundgren, and J. E. Greene, J. Appl. Phys. 84, 6034 (1998).

[32]. A.R. Smith, H. A. H. AL-Brithen, D. C. Ingram, and D. Gall, J. Appl. Phys. 90, 1809 (2001).

[33]. H. Al-Brithen and A. R. Smith, Appl. Phys. Lett. 77, 2485 (2000).

[34]. N. Takeuchi, Phys. Rev. B 65, 045204 (2002).

[35]. V. Ranjan, L. Bellaiche, and E. J.Walter, Phys. Rev. Lett. 90, 257602 (2003).

Appendix A.

The original Task 2 and four subtasks are listed here. If the year 1 subtasks were successful this would have been the subtasks that we would have completed in the second year.

Task 2 – Increase brightness of InScGaN and InYGaN based-LEDs (Second Year).

In Task 2, ScGaN and YGaN based MQWs and LEDs will be grown and emitting wavelengths will be determined using PL and electroluminescent "quick-tests" and full LED fabrication on select wafers. In addition, the optical emission intensity will be optimized for the alloys, and Sc and Y contents will be increased to produce the desired green, yellow, and orange wavelengths. This work will depend heavily on the results of the first year, so only general descriptions of this task are provided here.

Based on the linear extrapolation between the bandgaps, yellow emission might be achieved using 97% Sc and 46% Y, while the orange emission will only be reached at 50% Y content. After determining the alloy contents needed to achieve green and yellow emission, we will fabricate LEDs at these wavelengths. The electroluminescence wavelength and output power from "quick test" and full fabrication LEDs on select wafers will be reported. These results will be compared to conventional blue and green nitride-based LEDs currently fabricated at Sandia. After fabrication of green and yellow LEDs we will attempt to achieve an orange LED.

In this last task, indium will be added to the ScGaN and YGaN LEDs with the expectation that the internal quantum efficiency (IQE) will increase. For this work the growth temperature of the ScGaN and YGaN alloys will need to be lowered to incorporate between 5 to 10 % indium. If successful the high IQE currently that is currently observed for blue nitride based LEDs should be shifted to longer wavelengths.

In Task 2, ScGaN and YGaN based MQWs and LEDs will be grown and emitting wavelengths will be determined using PL and electroluminescent "quick-tests" and full LED fabrication on select wafers. In addition, the optical emission intensity will be optimized for the alloys and Sc and Y contents increased to produce the desired green, yellow, and orange wavelengths.

Subtask 2.1 Achieve ScN and YGaN with 50% Y.

To achieve the desired green, yellow and orange emission wavelengths, the Sc and Y contents in the alloys will need to be increased. Based on the linear extrapolation between the bandgaps, yellow emission might be achieved using 97% Sc and 46% Y, while the orange emission will only be reached at 49% Y.

Subtask 2.2 Demonstrate 530 nm (green) and 570 nm (yellow) LEDs using either ScGaN or YGaN active regions.

Following the work in Subtask 2.1, both green and yellow LEDs will be demonstrated. The electroluminescence wavelength and output power from "quick test" and full fabrication LEDs on select wafers will be reported. These results will be compared to conventional blue and green nitride-based LEDs currently fabricated at Sandia.

Subtask 2.3 Demonstrate a 590 nm (orange) or longer wavelength LED using YGaN active regions.

In this last subtask, the best quality, longest wavelength YGaN alloys will be incorporated into a GaN-based LED structure. Electroluminescence studies will be conducted to determine the

wavelength and the power output. These results will be compared to conventional blue and green nitride-based LEDs currently fabricated at Sandia.

Subtask 2.4 – Add Indium to the ScGaN and/or YGaN LEDs to increase the IQE.

In this last task, indium will be added to the ScGaN and YGaN LEDs with the expectation that the internal quantum efficiency (IQE) will increase. For this work the growth temperature of the ScGaN and YGaN alloys will need to be lowered to incorporate between 5 to 10 % indium. If successful the high IQE currently that is currently observed for blue nitride based LEDs should be shifted to longer wavelengths.

Appendix B. Brief Project Award Information

1 **DOE Award Number:** M6642867

2 **Project Title:** Novel ScGaN and YGaN Alloys for High Efficiency Light Emitters

3 **Performer:** Sandia National Laboratories, New Mexico

4 **Principal Investigator: Daniel D. Koleske**
Principal Member of the Technical Staff (PMTS)
Sandia National Laboratories, New Mexico
PO Box 5800
Albuquerque, NM 87185-1086
Phone Number: 505-284-4531 Fax Number: 505-844-3211
E-Mail: ddkoles@sandia.gov

5 **Other Team Members:**

Stephen R. Lee	Sandia National Laboratories, New Mexico
Mary H. Crawford	Sandia National Laboratories, New Mexico
J. Randall Creighton	Sandia National Laboratories, New Mexico
Gerald Thaler	Sandia National Laboratories, New Mexico
James A. Knapp	Sandia National Laboratories, New Mexico

6 **Technology Focus:** Core

7 **Relevant Subtask Priority Area:**
High-Efficiency Semiconductor Materials, 1.1.2 (Improve IQE across the visible spectrum and in the near UV – down to 360 nm)

8 **Schedule/Budget Overview:**

Budget Period	Start Date	End Date	Government Share	Performer Share	Total
1	(8/15/06)	(8/14/07)	$320,000	$ 0	$320,000
2	(8/15/07))	(8/14/08)	No cost extenstion	-	-
Total	**(8/15/06)**	**(08/14/08)**	**$320,000**	**$ 0**	**$320,000**

Distribution:

1	MS1086	Daniel D. Koleske	1126
1	MS1086	J. Randall Creighton	1126
1	MS1086	Karen C. Cross	1126
1	MS1086	Andrew A. Allerman	1126
1	MS1086	Robert M. Biefeld	1126
1	MS1086	Jeffrey J. Figiel	1126
1	MS1086	Stephen R. Lee	1123
1	MS1086	Mary H. Crawford	1123
1	MS1056	James A. Knapp	1111
1	MS0614	Michael J. Russell	2546
1	MS0899	Technical Library	9536 (electronic copy)